



http://pubs.acs.org/journal/acsodf Article

Interaction of the $(2\sqrt{3} \times 3)$ rect. Adsorption-Site Basis and Alkyl-Chain Close Packing in Alkanethiol Self-Assembled Monolayers on Au(111): A Molecular Dynamics Study of Alkyl-Chain Conformation

Soumya Bhattacharya, Mitchell P. Yothers, Liangliang Huang, and Lloyd A. Bumm*



Cite This: *ACS Omega* 2020, 5, 13802–13812



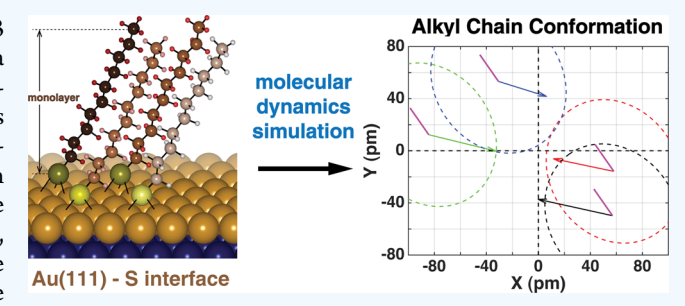
ACCESS

III Metrics & More

Article Recommendations

Supporting Information

ABSTRACT: We show that the adsorption site basis of the $(2\sqrt{3} \times 3)$ rect. phase of n-alkanethiol self-assembled monolayers plays a key role in determining the molecular conformation of the close-packed alkyl chains. Ten proposed reconstructed Au-S interfaces are used to explore the minimized energy alkyl-chain packing of n-decanethiol molecules using molecular dynamics with the all-atom description. In this comparative study, all models have the same alkyl-chain surface density of four molecules per unit cell; thus, differences are due to the headgroup spacing within the 4-molecule basis as opposed to the average surface density. We demonstrate for the first time the 4-molecule-basis twist structure driven by the



packing of alkanethiol molecules in a large simulation box (100 molecules, 25 unit cells) using molecular dynamics. Our results validate the prediction put forward by Mar and Klein that to achieve the 4-molecule-basis twist symmetry observed by the experiment, the headgroups must deviate from the high-symmetry $(\sqrt{3} \times \sqrt{3})R30^{\circ}$ sites. The key structural parameters: tilt, twist, and end-group height, as well as their spatial order, are compared with experimental results, which we show is a highly sensitive approach that can be used to vet proposed Au–S interfacial models.

INTRODUCTION

Alkanethiol self-assembled monolayers (SAMs) on Au(111) are one of the most widely studied ordered monolayer systems in the last 35 years¹ because of their potential applications in organic electronics,² nanotechnology,³ lithography,^{4,5} surface coating for corrosion prevention,⁶ chemical sensing,⁷ and many others.⁸⁻¹¹ A detailed understanding of the relationship between the properties of the SAM and the underlying structure is desired to fully harness their potential applications. The structure of saturation-coverage dense-phase SAMs is determined by the interplay between the alkyl-chain packing and Au-thiol adsorption interface. 12 The adsorption energy of the monolayer increases with increasing alkyl chain length because of interchain van der Waals (vdW) interaction which leads to crystalline order of the chains. 13-15 It is generally accepted that the herringbone reconstruction of bare Au(111)¹⁶ is lifted during SAM formation¹⁷ and that the surface undergoes a further complex reconstruction during SAM formation. However there is little consensus on the resultant Au-S interface structure beyond its $(2\sqrt{3} \times 3)$ rect. symmetry and four molecules per unit cell, which has led to a variety of proposed Au-S interface structures. 12,18

In this study, we chose 10 Au–S models and studied the alkyl-chain-driven SAM structures resulting from the adsorption site constraints. We used all-atom (AA) molecular dynamics (MD) models with *n*-decanethiol (C10). The

simulations begin with the Au-S interface in the postadsorption structures proposed in each of the 10 models. The Au and S atoms are static (not allowed to move) in this MD study. Only the alkyl chains are allowed to relax during the simulation. The Au-S-CH₂ bond-bending potential is set to zero which allows the S-CH₂ bond to adopt any orientation with respect to the surface, controlled only by the relaxation of the rest of the system. This approximation for the C10 molecule is reasonable as demonstrated by previous studies. 19-21 The SAM structures we present represent those that provide the best alkyl chain packing, given the constraints of adsorption sites. Prior MD studies reported a 1-molecule basis structure for headgroups constrained in $(\sqrt{3} \times \sqrt{3})R30^{\circ}$ adsorption sites, where all the chains adopt the same twist. 22-24 In contrast, experiments have observed at least two nearly orthogonal chain twists per unit cell arranged in a 4molecule-basis zig-zag structure. 25-27 In order for multiple chain twists to emerge for close-packed molecules, the headgroups must deviate from the high symmetry ($\sqrt{3}$ ×

Received: March 12, 2020 Accepted: May 20, 2020 Published: June 2, 2020





 $\sqrt{3})R30^\circ$ sites within the $(2\sqrt{3}\times3)$ rect. unit cell. This requirement was first proposed by Mar and Klein. ²¹ Although the molecular packing is known to be sensitive to the symmetry and the separation of the headgroups, ^{28,29} multiunit cell MD simulations using $(2\sqrt{3}\times3)$ rect. reconstructions have not been studied for medium and long chains. We choose $10~\mathrm{Au-S}$ interface models to study Mar and Klein's conjecture and compare other structural parameters with experimental observations. Our result shows that the vdW-driven close packing of the chains leads to significantly different SAM structures depending on the Au–S interfaces.

This well-known sensitivity of the alkyl chain structures to the headgroup spacing also can be exploited as a method for examining proposed Au-S interface models. We compare the SAM alkyl chain geometries obtained from the energyminimized MD simulation with experiment. Ab initio methods have been used to study the Au-S interface and have proposed a variety of structures for short alkyl chains. However, the technically interesting SAMs are made using alkyl chains with eight carbon atoms and longer, where the chain packing is a major component of the adsorption energy. 13 Most of the experimental work has been performed on these longer chain SAMs. The complexity of the Au-S interface combined with the critical importance of the vdW energy, and the number of atoms that would need to be included for longer chains, makes the full problem beyond the reach of ab initio methods. In this work, we demonstrate an approach for comparison of proposed Au-S interfaces to experiment via MD simulations of the alkyl-chain packing structures which bridges this computational gap. We are not aware of any comparable studies of the long-chain (C10) alkanethiol molecules in largescale simulation (≥100 molecules) over 100 ns on the reconstructed $(2\sqrt{3} \times 3)$ rect. unit cell of the Au–S interface.

The key structural parameters of the molecules in the SAM tilt (θ) , twist (φ) , and tilt direction (χ) are defined in Figure 1 for the molecule in the idealized all-trans conformation. The tilt direction is defined with respect to a reference direction on the surface (x-axis in Figure 1) which is typically the Au $\langle 110 \rangle$ direction and nominally the next-nearest-neighbor (NNN) direction in the SAM (in this work we use [110]; see Figure 2). The molecular axis for an all-trans chain bisects the C-C bonds, Figure 1. The molecular axis is defined as the best-fit line to the midpoints of the C-C bonds. The twist angle is defined as the rotation of the plane of the carbon atoms around the molecular axis (molecule's long axis) and is right-handed with respect to the axis originating on the surface. The twist angle zero is defined as the angle, where the molecular plane and the tilt plane coincide, and the alpha methylene is closest to the surface. These angles are most structurally descriptive for chains that are close to the all-trans conformation that have a well-defined molecular backbone plane.

Interface Models. Several models of the atomic structure of the Au–S interface have been proposed based on the experimental results, which was sometimes accompanied by atomistic modeling. In other models, ab initio methods are used to find minimized energy structures of the Au–S interface. Most of these models contain adatoms and/or vacancies, and their surface coverage is quantified with respect to the substrate Au atoms. The unreconstructed Au(111) surface $(2\sqrt{3} \times 3)$ rect. unit cell contains 12 Au atoms. An integer number of adatoms or vacancies per unit cell correspond to fractional coverages of adatoms and vacancies $(\theta_{\rm ad}$ and $\theta_{\rm vac}$, respectively) in multiples of 1/12 (~0.083). For

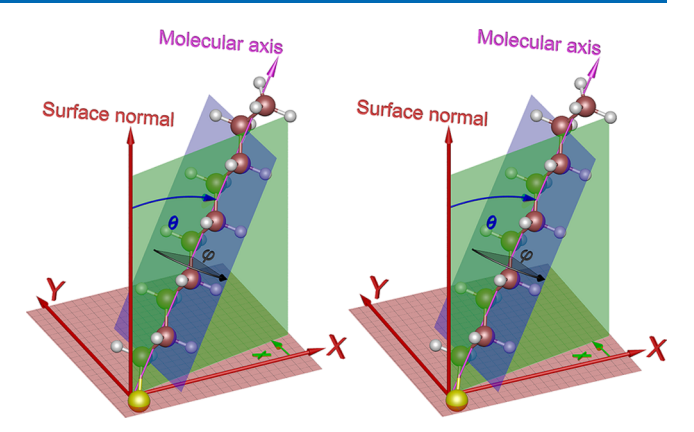


Figure 1. Parallel stereo image pair of the molecular geometry. In this alkyl-chain centric model, the molecular axis passes through the origin, where it intersects the surface. The tilt angle (θ) is defined by the angle between the surface normal (z-axis) and the axis of the molecule (molecular axis). The twist of the molecular backbone (φ) is defined by the angle between the tilt plane (green plane) containing the surface normal and the molecular axis and the plane of the alkyl carbon atoms (blue plane). A zero twist angle is defined where these two planes coincide and the bond between the headgroup and the alpha methylene makes the largest angle with respect to the surface normal (α -CH₂ is closer to the substrate). A positive increasing twist angle is defined in the counterclockwise direction while looking down the molecular axis toward the surface as is the standard for a righthanded coordinate system. The direction of the tilt (χ) is the angle between the positive x-axis and the projection of the molecular axis on the plane of the substrate (xy-plane).

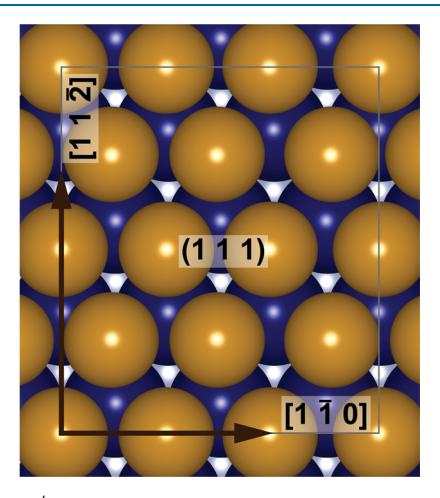
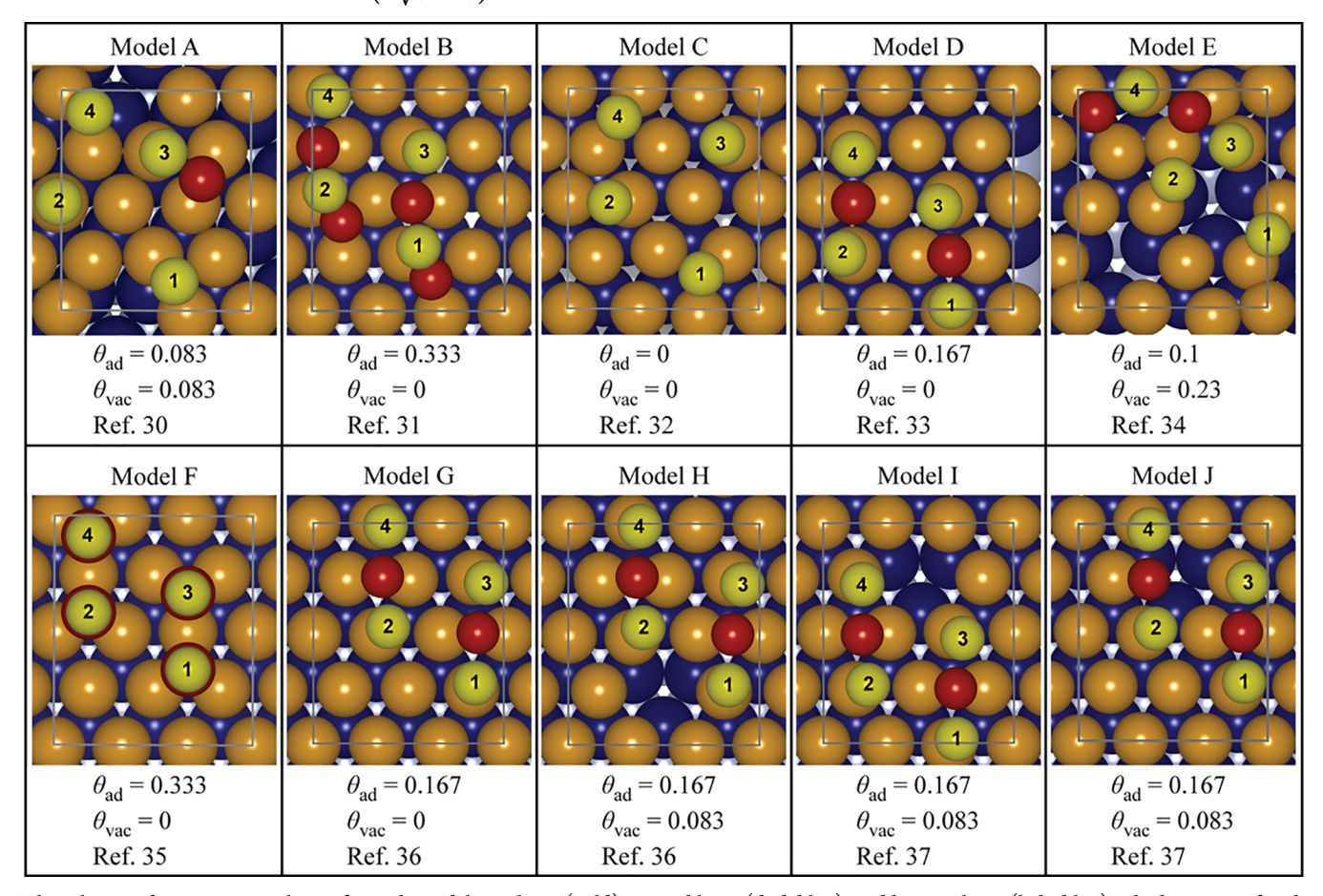


Figure 2. $(2\sqrt{3} \times 3)$ rect. unit cell shown on an unreconstructed Au(111) surface. The six $\langle 1\ 1\ 0\rangle$ directions are symmetry-equivalent for the unreconstructed Au(111) and the $(\sqrt{3} \times \sqrt{3})$ R30° overlayer. The $(2\sqrt{3} \times 3)$ rect. in general renders all six $\langle 1\ 1\ 0\rangle$ directions inequivalent, depending on the symmetry of the basis.

example, model F (Table 1) is proposed based on a symmetry argument to explain the LEED pattern observed from butanethiol SAMs. In this model, the headgroup is attached on top of an adatom ($\theta_{\rm ad}=0.333$) which is connected to the substrate at the fcc or hcp hollow site with no surface vacancy per unit cell ($\theta_{\rm vac}=0$). In contrast, models B, C, and D were proposed based on the ab initio calculations alone while comparing with the other Au–S interface models. In these models, $\theta_{\rm ad}=0$, 0.167, and 0.333 for C, D, and B, respectively. Ab initio methods also have been employed to develop models used to fit GIXRD or STM experimental

Table 1. Atomic Structure of the $(2\sqrt{3} \times 3)$ rect. Unit Cell for 10 Au–S Interfacial Models



Three layers of Au atoms are shown for each model: top layer (gold), second layer (dark blue), and bottom layer (light blue). The basis site of each S atom (yellow) is identified by a number. The Au adatoms (red) and the vacancies per unit cell are given as a fraction of the surface Au atoms in an unreconstructed Au(111) substrate, containing 12 Au atoms in $(2\sqrt{3}\times3)$ rect. unit cell. The subsurface Au layers are depicted as unreconstructed Au(111) for models A and D because their coordinates were not published. The unit cell for model C and I were rotated 180° to be consistent with the underlying crystal structure of the rest of the models. The subsurface layers of Au(111) are shown to visualize the fcc and hcp hollow sites.

results. For example, Cossaro et al. proposed model E as the best fit model to the GIXRD measurements of the hexanethiol SAMs.³⁴ The complex reconstructions in models D, G, H, I and I are strikingly similar, each with a two staple motifs oriented in the long axis of the unit cell. The latter three have one Au substrate vacancy per unit cell. The complex reconstruction in model E shows the coexistence of the extended staple motif and the adsorption of the headgroups at the bridge sites with fractional occupancies per unit cell (θ_{ad} = 0.1 and $\theta_{\rm vac}$ = 0.23). For our study, we used the fixed occupancies shown in the model E diagram ($\theta_{\rm ad}$ = 0.167 and $\theta_{\rm vac}$ = 0.167). The motivation for the other five models (A, G– J) was to reproduce the 4-molecule-basis surface structure observed in STM. ^{30,36,37} Apart from models A, C, and F, all the models have two adatoms per unit cell ($\theta_{ad} = 0.167$), and models A, H, I, and J have one surface vacancy per unit cell $(\theta_{\rm vac} = 0.083).$

The sulfur adsorption sites in these 10 models are all offset from the high symmetry ($\sqrt{3} \times \sqrt{3}$) $R30^{\circ}$ sites of a simple close-packed overlayer. In other words, the adsorption sites are not uniformly spaced within the unit cell. Although this is an obvious consequence of the lower ($2\sqrt{3} \times 3$)rect. translational symmetry with a 4-molecule basis, it is significant because the

alkyl chains prefer a close-packed lattice. Our work is the first classical MD study of the effect of sulfur headgroup offsets on the alkyl chain structure. Our approach is quite different from the $(\sqrt{3} \times \sqrt{3})R30^{\circ}$ Au-S adsorption sites of the unreconstructed surface generally used in the MD studies. 21-24,39 The deviation of the headgroup from $(\sqrt{3} \times \sqrt{3})$ R30° sites in these 10 models is critical for stabilizing the nontrivial twist structures observed in experiment. This is the first demonstration where a 4-molecule-basis twist structure has emerged spontaneously in an MD simulation. The selected 10 Au-S interfacial models are shown in Table 1. The coordinates for the sulfur headgroups and adatoms are given in the Supporting Information. The rest of the paper is organized as follows: we first compare the structure of the SAMs for different interfacial models with the experimental results, examine the effect of the headgroup basis on the alkyl chain conformations, and then present the details of the MD modeling.

RESULTS AND DISCUSSION

In order to examine the influence of the adsorption site basis, we need to examine each of the alkyl chain structural parameters. It is also instructive to compare the resulting

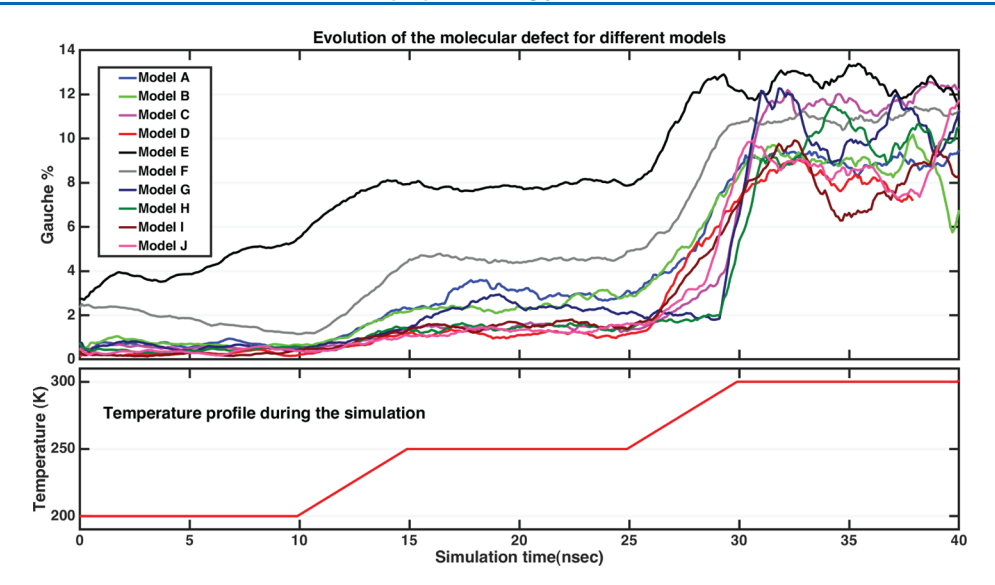


Figure 3. Average gauche fraction (%) of models (A-J) compared at 200, 250, and 300 K. Note that it rises above 5% for 300 K for all models.

alkyl chain geometry from the chain packing alone with experimental observations to speculate which proposed Au-S interfacial structure is the best match. In our MD study, the gold and sulfur atoms are fixed in the positions defined by each model. Thus, our study does not include surface diffusion and/ or desorption of the molecules which would occur at temperatures above those of interest for the well-ordered SAMs in this study. In particular, we use these models to reproduce the structure of the monolayer at room temperature and below, where the monolayer is crystalline, and the alkyl chains are predominantly in the all-trans conformation. Four symmetry inequivalent adsorption sites per unit cell is a general feature of the proposed models which may also include Au adatoms and/or Au vacancies. These models allow us to study the structural effects not only of different adsorption sites but also because of the presence of adatoms and vacancies. The resultant monolayer was evaluated for each model using the structural parameters (height, twist angle, tilt angle, tilt direction, and gauche fraction), their spatial patterns, and the thermal stability of the SAM. We also comment how well each of the models reproduces the experimentally measured structural parameters. The rest of the section is organized as follows: first, we study the dependence of the average gauche fraction on simulation temperature and its impact on the tilt angle, and then, we analyze the height of the molecules, the molecular twist, the tilt direction, and the thermal stability of the resultant structures. With these, we can examine the effect of the adsorption site offset on the geometry of the closepacked alkyl chains.

The alkyl chains are known to be predominantly in the all-trans conformation at room temperature from infrared reflection absorption spectroscopy (IRRAS). ^{26,40,41} Both infrared measurements and MD simulations show that the conformational order decreases with decreasing chain length and decreases with increasing temperature. Most of the gauche defects are concentrated near the methyl termini at 300 K but penetrate deeper into the monolayer as the temperature is increased. ²¹ The deviation from all-trans can be quantified by the gauche fraction, defined in the Supporting Information. Conformational defects in the alkyl chains can significantly influence the structure of the monolayer. Disorder in the alkyl chain reduces the volume density because increasing gauche

fraction effectively increases the diameter of the chain (becoming shorter and fatter) evolving toward a random coil in the limiting case. Hence, for a fixed surface density of molecules, the fatter the chain becomes, the smaller the tilt angle becomes. For modest temperatures of interest in our study, the effect of gauche defects is to slightly decrease the tilt angle of the chains.

Our simulations show that gauche defects in the alkyl chains increase with rising temperature as expected. Figure 3 shows that the average gauche fraction for the temperatures used in this study (200, 250, and 300 K) exceeds 5% for $T \ge 300$ K for all models. In particular, the gauche fraction for model E is significantly larger than the other models. This indicates that the monolayer structure predicted by model E might be unstable (discussed in detail later in this section). The increase in the gauche fraction occurs at lower temperatures than found in an earlier study,²¹ which we attribute to the chosen force field (FF). (The problem of transferability of the FF parameters.) The experimentally observed disorder at room temperature correlates with a gauche fraction <2%,42 which matches most closely with our 200 and 250 K simulations. In addition, because the gauche fraction and the tilt angle are related, the higher gauche fraction at 300 K in these models drives the tilt angles to be too small for meaningful comparison with experiments (less than 25° for all models at 300 K). Therefore, we will focus our discussion on 200 and 250 K simulation results as the most representative of the experimental system at room temperature.

The height of the terminal methyl groups and the symmetry of their arrangement at the outer surface depends on the details of the atomic structure at the Au–S interface. We define the height of the molecule as the distance of the methyl carbon above the plane of the nominal Au(111) surface atoms. Constant current STM images of alkanethiol SAMs show different phases of the 4-molecule-basis surface symmetry with a height difference between the lowest and the highest basis type ranging from 50 to 90 pm. 43,44 We compare our simulation results with the experimental observations keeping in mind that our model shows the physical height difference between the basis types, whereas the STM height difference is a convolution of the physical height with molecular conductivity. Figure 4 shows the spatial distribution of the

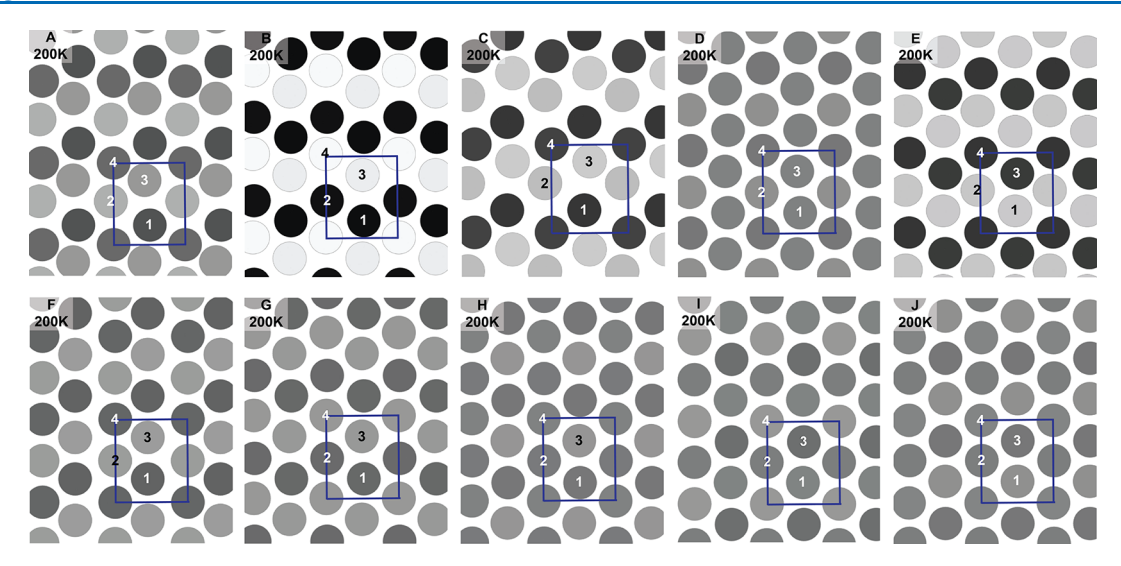


Figure 4. Spatial symmetry of the molecular height at the methyl interface at 200 K for models (A–J). The numbering scheme for the basis types is the same as in Table 1. For better visualization, the $(2\sqrt{3} \times 3)$ rect. unit cell (blue box) is tiled 3×3 for easy visualization of the patterns. The position of the circles is the average position of the methyl groups, and the color of the circle represents the average height of the molecule. The higher molecules are represented by the lighter shades.

average height at 200 K for the 10 models, where the height of a molecule is averaged over both the simulation time for a given temperature and over the basis type. (See Figure S4 for 250 K simulation results.) All the models exhibit a 4-molecule basis in height difference similar to the STM result. Models D and J exhibit height differences significantly smaller than the other models which are too small to reproduce the STM observations on physical height alone. Although small, these height differences are statistically significant and exhibit a 4-molecule basis. In summary, models D and J are unlikely candidates to represent the real SAM structure.

The relative height of a basis type depends both on the molecular geometry and the height of the corresponding headgroup from the substrate. To understand the influence of these separately on the height of a molecule, we divide the physical height of a molecule into the height of the sulfur headgroup from the substrate and the height of the methyl carbon from the corresponding sulfur atom. Figure 5 shows the average height of each basis type for all the models at 200 K. The largest contributor to the height difference is the sulfur adsorption site, which can be seen directly in the heights of the corresponding terminal methyl groups (models B, C, and E). Model B exhibits a particularly strong height difference 152 ± 7 pm enforced by the underlying adsorption sites. On the other hand, the sulfur atoms for model F are all at the same height from the substrate yet the methyl height difference is distinct. Therefore, the height difference between the basis molecules in model F is only because of the differences in the molecular conformation: the molecular twist and the averaged gauche defects. We also studied the temperature dependence of the molecular height and found that the height of the molecules at 250 K is higher than at 200 K, Figure S5, which is a manifestation of the decrease in tilt angle. The tilt angle is closely associated with order and the density of the monolayer, with all-trans chains packing most efficiently forming the largest tilt angles (25-35°) and highest volume density. 26,45,46 We conclude that the height of a molecule is determined by a combination of the corresponding sulfur adsorption site and the molecular conformation.

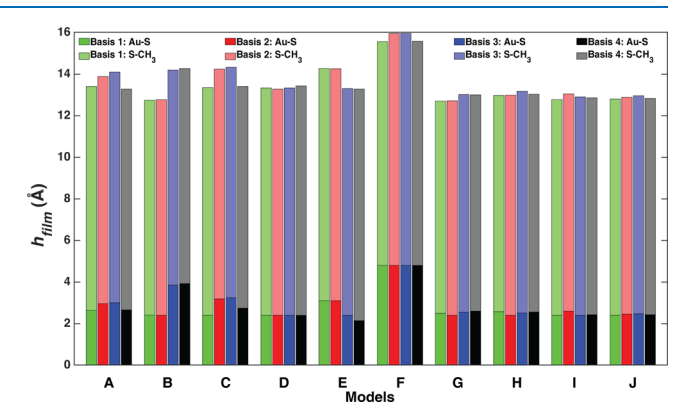


Figure 5. Average height of the four basis-type methyl-group C atoms from the Au(111) substrate for each model are separated by contribution. The darker segments (Au–S) represent the z-height of the S headgroups from the Au(111) substrate, the contribution to the z-height from the S atom adsorption site. The lighter segments (S–CH $_3$) represent the z-height of the methyl group C atoms from the corresponding S atoms, the contribution to the z-height from the molecular conformation.

The alkyl chain twist is the most sensitive of the structural parameters, thus providing an important comparison with the experiment. Experimental IRRAS measurements show two equal populations of near mutually orthogonal chain twists per unit cell, 50 and 132°.47 (See the Supporting Information for detailed discussion.) Because IRRAS measures the surface normal component of the transition dipole moment, these measurements cannot distinguish between angles with mirror symmetry about the plane of the molecular tilt (Figure 1). Therefore, for comparison of the IRRAS results, we have used this mirror symmetry to fold the $0-360^{\circ}$ twist angles into the interval 0-180°, which we designate as the folded twist. Each unit cell could contain two, three, or four different twist angles and satisfy the experimental observations. In MD simulations of SAMs, four distinct twist angles can be observed at temperatures, where there is some twist disorder indicating that these are local energy minima for alkyl chain packing. ^{21,48} One twist angle occurs in each of the four quadrants in the

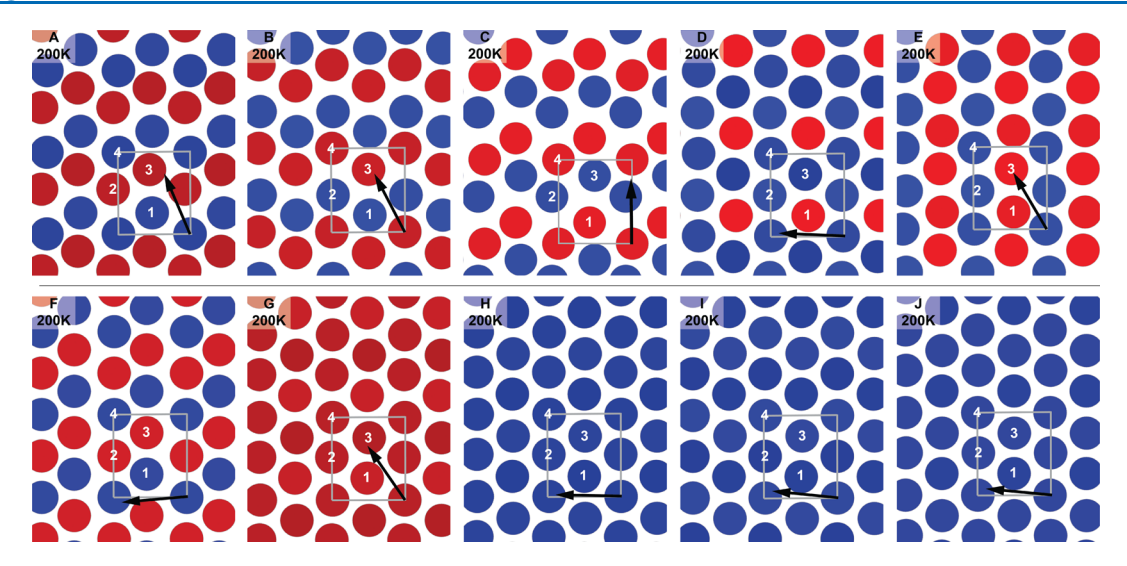


Figure 6. Spatial distribution of the molecular twist is shown for 10 Au–S interfacial models at 200 K for models (A–J). The position of the circles is the average position of the methyl groups, and the color of the circle represents the average value of the folded twist; blue: $0^{\circ} \le \phi < 90^{\circ}$ and red: $90^{\circ} \le \phi < 180^{\circ}$. The corresponding tilt direction (black arrow) and the $(2\sqrt{3} \times 3)$ rect. unit cell (gray rectangle) are shown for comparison. The numbering scheme for the basis molecules is the same as in Table 1. The $(2\sqrt{3} \times 3)$ rect. unit cell is tiled 3×3 for easy visualization of the patterns.

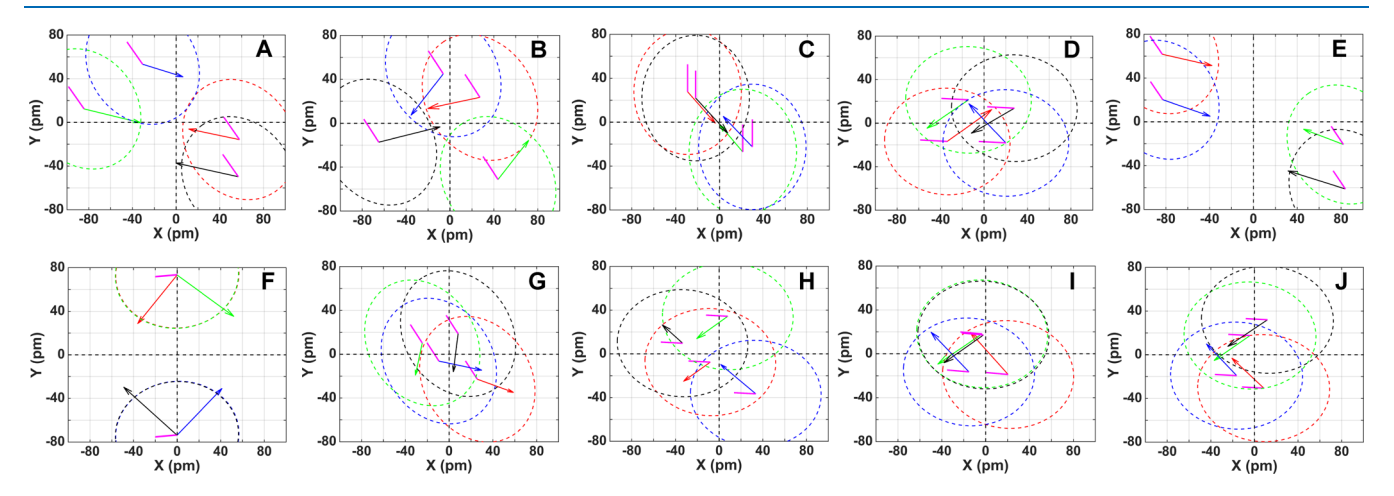


Figure 7. Comparison of the SAM sulfur adsorption sites and alkyl chain molecular geometry for the models (A–J). The locations are shown in the reference frame of the RCP coordinate system (see the text). The S headgroup positions are at the vertex of the arrow and the magenta lines. The chain axis is located at the end of the arrow. The magenta lines for each arrow indicated the chain tilt direction. The twist is the angle between the magenta line and the arrow. The dotted ellipses show the possible positions of the idealized all-trans alkyl chain axis as the twist is swept in a full circle around the S headgroup. The basis types are indicated by the color of the arrows (red = 1, green = 2, blue = 3, and black = 4).

range 0-360°. These collapse into two quadrants in the folded twist shown color-coded in Figure 6, first quadrant 0-90° (blue), and second quadrant 90-180° (red). The average twist of a basis molecule is evaluated by the spatial average over the basis type as well as time average for a given temperature. Figure 6 shows the spatial distribution of the average twist for all the models at 200 K; similar plots are given in the Supporting Information at 250 K (Figure S7). At 200 K, models A, B, C, E, and F exhibit two twists >90 and two less than 90° per unit cell. Models G, H, I, and J exhibit a single twist angle. Model D exhibits two twist angles with a population of three to one. The twist angles for model B are 72 ± 6 and $110 \pm 6^{\circ}$, which are not orthogonal to each other. Therefore, models B, D, G, H, I, and J do not exhibit the correct twist characteristics. This leaves models A, C, E, and F consistent with the experimental IRRAS measurements.

We also compare the models using the tilt direction and their thermal stability. The tilt direction of the molecules in an ordered SAM should be along the NNN direction to optimize the interchain vdW interaction.⁴⁹ We have observed that crowding of the headgroups, such as in models C and E, has a significant effect on the tilt direction and the thermal stability of the SAMs. For instance, the average tilt direction for model C is toward the nearest neighbor (NN) direction for both 200 K (Figure 6) and 250 K (Figure S7). Although molecules are tilted toward their NNN direction in model E at 200 K, the direction changes to a symmetry inequivalent direction with increasing temperature (see Figures 6E and S7E). Moreover, the spatial distribution of the twist has a 2-molecule basis surface structure at 200 K which is changed into a 4-molecule basis at 250 K. Combined with the anomalously high gauche fraction already discussed, the change in the tilt direction and the symmetry of the twist with respect to the temperature indicates that model E is unlikely to represent the observed structure of the monolayer. As a result, models C and E are

Table 2. Comparison of the rms Deviation of the Sulfur Headgroups (a_S) and the Alkyl Chain Axes (a_C) from the Close-Packed Lattice for Models (A-J)

model	A	В	C	D	E	F	G	Н	I	J	$(\sqrt{3} \times \sqrt{3})R30^{\circ}$
$a_{\rm S}$ (pm)	142.8	111.8	71.8	61.3	189.8	147.0	49.4	76.2	43.8	67.2	0
$a_{\rm C}~({\rm pm})$	10.6	10.9	8.7	9.4	36.1	34.6	8.7	8.5	10.6	8.7	8.4
$\sigma_{\rm C}~({ m pm})^a$	2.4	2.3	3.2	2.9	6.9	6.9	3.3	3.3	3.2	3.2	2.1

^aThe standard deviation of the alkyl chain axes are also tabulated (σ_C).

probably not good candidates to represent the n-decanethiol SAM.

Finally, we study the relationship between the basis site offset from the high symmetry $(\sqrt{3} \times \sqrt{3})R30^{\circ}$ basis sites and the resultant geometry of the alkyl chains driven by their close packing, particularly, chain tilt direction and chain twist. First, we must remove a complication that arises because the sulfur adsorption sites in these models are not only offset from their ideal basis sites but also have different basis heights above the nominal substrate plane (Figure 5). Height differences of the sulfur sites translate to a difference in lateral spacing of the alkyl chains in the tilt direction. In order to accurately compare the offsets, the adsorption sites and alkyl chain axes must be referenced to a common plane. For our analysis, the position of the headgroups are projected along the alkyl chain axis to a common plane parallel to the unreconstructed Au(111) substrate plane. The position of the alkyl chain axis is taken as the point where it intersects this plane. Now, we can define a reduced coordinate system with respect to the associated closepacked lattice and the high-symmetry $(\sqrt{3} \times \sqrt{3})R30^{\circ}$ sublattice of the $(2\sqrt{3} \times 3)$ rect. unit cell. For simplicity, we choose an origin of the close-packed lattice such that the four offset vectors sum to zero. To achieve this, we first align the unit cell origin with one of the adsorption sites. The offset vectors of the four sites to the corresponding $(\sqrt{3} \times \sqrt{3})R30^{\circ}$ sublattice sites are determined. The sum of the offset vectors is the position of the best-fit unit cell origin. The unit cell origin is then translated to the new coordinate frame. Rotation is not allowed because that would violate long-range translational symmetry. The resulting offset vectors are in a reduced closepacked (RCP) coordinate system.

Figure 7 shows the resulting SAM structures for each model in the RCP coordinate frame. The headgroup offset for each basis site is represented by origin of the arrows and are colored to identify each basis type. The root-mean-square (rms) average offset for the four basis sites (a_s) , a measure of the deviation from the close-packed lattice, is given in Table 2. The possible locations of the chain axis, in the case of ideal all-trans alkyl chains, trace out an ellipse around each sulfur that is elongated in the tilt direction (see Supporting Information and Figure S2). The average position of the molecular axes in the simulations is at the tip of the arrows. The molecular twist is the angle between the tilt direction (magenta line) and the arrow. For further analysis, we shift the origin of the coordinates for the alkyl chain axes such that the sum of their offset vectors is zero, as we did for the sulfur headgroups and report the rms average offset (a_C) and standard deviation (σ_C) of the four-basis-site chain axes in Table 2. The standard deviation is a measure of the stability and fluctuation of the chain axis fit during the simulation time. A larger standard deviation indicates a higher gauche fraction. The simulation results for a reference structure with the sulfur headgroups in $(\sqrt{3} \times \sqrt{3})R30^{\circ}$ sites on the unreconstructed Au(111) substrate at 200 K is included for comparison.

Table 2 clearly shows that in all 10 models, the headgroups are offset from a close-packed lattice and the alkyl chains adjust to reduce that offset. The propensity for the chains to closely pack is also evident in Figure 7 from the tendency of the chain axes to be more tightly clustered than the headgroups. However, none of the models allow perfect packing of alltrans alkyl chains. If this were possible, the four chain-axis ellipses would intersect with each of the alkyl chain twists close to one of the four optimum twist angles. The chains can adapt to adverse headgroup packing by adding gauche defects near the surface, thereby facilitating the remaining portion of the chain to adopt a more optimal close-packed geometry. For example, model E has the largest headgroup rms average offset (a_S) and the alkyl chains achieve the poorest close packing, as shown by the highest $a_{\rm C}$ and $\sigma_{\rm C}$. This is consistent with the significantly higher gauche fraction observed in the simulations compared to the other models. In contrast, the reference structure where the sulfur headgroups were exactly in closepacked sites (Table 2) allows better close packing of the chains than any of the 10 models studied, as evidenced by the smallest $a_{\rm C}$ and $\sigma_{\rm C}$. Visualizing this structure in the RCP coordinate frame in Figure S8 shows that the alkyl chains adopt a single twist. All four headgroups are at the origin with identical overlapping ellipses (Figure S8). The chain axes all fall close to the same point on the ellipse. The small deviation is because of the thermal gauche defects. Models F and A have the next highest a_S , but their a_C are strikingly different. Model A allows the alkyl chains to achieve better close packing, with model F exhibiting $a_{\rm C}$ and $\sigma_{\rm C}$ over three times larger. Graphically, models A, C, E, and F show a clear propensity for the molecular axes being more tightly clustered than their headgroups (Figure 7). Although that trend is less apparent for the rest of the models, it is very evident from the σ_C values. It is interesting that the chain packing as quantified by a_C are all similar except for models E and F. The models where the chain axes fall nearer to the ellipses exhibit a smaller σ_{C_r} as expected. The value of a_C for all the models except model E and F is comparable to the reference structure, indicating that they achieve an ordered close-packed SAM structure.

The extreme sensitivity of the alkyl chain conformation to the headgroup spacing is well illustrated by the models D, G, H, I, and J which are visually very similar but have distinct headgroup offsets in the RCP coordinate frame. These lead to very different chain twist combinations, and in the case of model G, a different tilt direction than the other four. The $a_{\rm C}$ and $\sigma_{\rm C}$ values of the five models are very close, indicating that the efficiency of the chain packing is similar.

Figure 7 illustrates how multiple twist combinations arise as a natural consequence of the basis site offset of the sulfur headgroups from ideal close-packed sites. For example, in model A, the alkyl chains adjust to optimize their close packing by adjusting the chain twist (and tilt) to bring the chain axes closer together. Without the headgroup offset, neighboring

Table 3. Comparison between Simulation and Experimental Results for Models (A-J)

	model	T (K)	tilt angle (deg)	tilt direction ^a (deg)	twist $angle^b$ (deg)	Δh (pm
simulation	A	200	32 ± 1	5.26 ± 2.37	$(46 \pm 5), (139 \pm 5)$	81.5
		250	26 ± 1	6.62 ± 3.17	$(49 \pm 10), (138 \pm 10)$	87.8
	В	200	36 ± 1	3.27 ± 0.492	$(72 \pm 6), (110 \pm 6)$	151.9
		250	32 ± 2	0.876 ± 0.478	$(75 \pm 7), (108 \pm 9)$	143.4
	С	200	31 ± 1	29.5 ± 1.40	$(39 \pm 5), (140 \pm 5)$	98.7
		250	29 ± 1	29.3 ± 1.38	(137 ± 7)	101.1
	D	200	32 ± 1	3.26 ± 1.79	$(40 \pm 5), (135 \pm 5)$	19.3
		250	28 ± 3	1.83 ± 1.39	$(43 \pm 6), (136 \pm 7)$	19.1
	E	200	30 ± 2	4.46 ± 5.53	$(43 \pm 6), (143 \pm 8)$	99.3
		250	21 ± 3	3.95 ± 4.39	$(47 \pm 12), (137 \pm 12)$	81.1
	F	200	30 ± 1	5.12 ± 2.12	$(47 \pm 5), (139 \pm 5)$	42.9
		250	25 ± 1	6.94 ± 2.41	$(51 \pm 9), (137 \pm 9)$	39.2
	G	200	36 ± 1	3.19 ± 0.770	(141 ± 5)	31.4
		250	32 ± 1	4.38 ± 0.854	$(46 \pm 7), (140 \pm 7)$	27.1
	Н	200	35 ± 1	2.65 ± 1.15	(42 ± 5)	19.9
		250	33 ± 1	2.61 ± 1.15	$(45 \pm 7), (139 \pm 7)$	17.4
	I	200	35 ± 1	5.26 ± 1.51	(41 ± 5)	27.6
		250	33 ± 2	6.22 ± 1.16	(42 ± 6)	25.7
	J	200	36 ± 1	3.26 ± 1.22	(41 ± 5)	15.7
		250	33 ± 1	2.53 ± 1.08	$(42 \pm 7), (140 \pm 7)$	9.9
experimental			$25-35^{26}$	NNN ^{25,27}	50, 132 ⁴⁷	~90 ⁴⁴

"The direction of the tilt angle is shown in Figure 6. The angle is a measure from the NNN direction. "The twist angles are calculated for the folded twist; see the text for more details. "The maximum height difference between the molecular heads measured in STM depends on the tunneling conditions, the nature of the bonding of the headgroups to the substrate, and the length of the molecules because the STM image is a convolution of the physical height and the electronic properties of the molecules. Here, we are reporting only the maximum physical height difference (Δh) between the basis methyl carbon atoms. Therefore, the discrepancy between the experimental and the simulated values can be attributed to the excluded electronic effects of the molecule.

chains cannot adopt different twists without conflict. This requirement was first proposed by Mar and Klein.²¹

Models A and F reproduce all the experimentally observed structural parameters of height difference symmetry, tilt direction, and chain twist. Model A exhibits two chain twists and model F exhibits all four. The alkyl-chain packing is not as optimal in model F, and as such, displays more disorder. Model A is the best candidate based on the chain packing. We have eliminated models D and J because the resulting molecular height symmetry is not a 4-molecule basis. Models B, D, G, H, I, and J do not produce an equal population of orthogonal molecular twist angles. We eliminate model C because the molecules tilt toward the NN instead of NNN. These results (Table 3) demonstrate that the SAM structure is quite sensitive to the Au-S interface.

CONCLUSIONS

Most of the recent efforts to understand the structure of SAMs have focused on the Au-S interface and models for the complex reconstruction of the Au(111) surface. This body of work has resulted in a wide variety of $(2\sqrt{3} \times 3)$ rect. unitcell models for the reconstructed Au-S interface. However, a simplified $(\sqrt{3} \times \sqrt{3})R30^{\circ}$ adsorption geometry of the interface is commonly considered for the MD simulation. We have shown how the headgroup deviation from the idealized $(\sqrt{3} \times \sqrt{3})R30^{\circ}$ sites strongly affects the geometry of the chains. We chose 10 complex reconstructions of the Au-S interface for our study. From these, we have constructed models of C10 SAMs and compared the resulting monolayer with experimental measurements of the alkyl chain structure. The pattern of molecule heights at the outer surface was compared to STM images. The tilt, twist, and tilt directions of the molecular backbone were compared to IRRAS measurements. Deviation of the headgroup from the ideal sites in these reconstructed models drives the molecules to obtain different twists for efficient packing. This results in equal population of at least two nearly orthogonal twists for models A, B, C, E, and F that is consistent with the IRRAS observation. This is the first report of a 4-molecule-basis twist structure emerging in MD simulations that is consistent with experiment. Two of the 10 Au-S structures considered (models A and F) reproduced all the experimentally observed alkyl chain structure parameters despite all models having the same alkanethiol coverage.

Our model can be improved with realistic potentials for Au-S-CH₂ bond bending and dihedral for the low symmetry adsorption sites prevalent in the Au-S models. An AA FF trained for SAMs would be advantageous, although sensible results are obtained with simple temperature scaling. It is important to note that SAMs have application at higher temperatures where the crystalline order diminishes. 3,50,51 It was not the intent of this work to promote any particular structure as correct or incorrect because these results may also be sensitive to the Au-S-CH₂ bond potential. Our study underscores the value to develop the crucial MD FF parameters at the Au-S interface for more realistic simulation of the SAM structure.

METHODS

The MD simulations of C10 SAMs were preformed utilizing the LAMMPS⁵² MD package using the velocity-Verlet algorithm and AA FF (OPLS-AA⁵³). The structure of the FF is given below, with the values of the parameters tabulated in the Supporting Information.

$$E = 4\varepsilon \left\{ \left(\frac{\sigma}{r} \right)^{12} - \left(\frac{\sigma}{r} \right)^{6} \right\} + C \frac{q_i q_j}{\varepsilon_0 r} + K_r (r - r_0)^2$$

$$+ K_\theta (\theta - \theta_0)^2 + K_\phi^{-1} (1 + \cos \varphi) + K_\phi^{-2}$$

$$(1 - \cos 2\varphi) + K_\phi^{-3} (1 + \cos 3\varphi)$$

The first two terms on the right side of the equation represent the nonbonded interaction, vdW (Lennard-Jones), and Coulombic potential, respectively. The third and the fourth terms are for the harmonic vibration of the bond stretching and the bond bending, respectively. The last three terms are the first three Fourier components of the dihedral angles. The higher-order Fourier components of the dihedral were not used in the OPLS-AA dihedral potential for alkanes. Note that the AA description of the molecules is required to correctly model the alkyl chain twist in the SAMs; the simpler united atom description does not model the twist correctly. 21,22,54

A simulation box with 5×5 ($2\sqrt{3} \times 3$) rect. unit cells (100) molecules) was used. The Au and S atoms were fixed; only the alkyl chains were allowed to relax. The Au-S-CH, bond bending potential is set to zero so that the orientation of the S-CH₂ bond will be determined by the alkyl chain packing. To find the equilibrium structure of the SAMs, we started with all 100 C10 molecules (all-trans) standing perpendicular to the substrate with zero tilt and zero twist angle (for the molecular geometry, see Figure 1), with periodic boundary conditions applied to the simulation box of dimension 43.2563 Å × 49.9481 Å. The structure is relaxed under the NVT ensemble over 10 ns using the Nose-Hoover thermostat at 200 K with a 1 fs time step. We found that relaxing the SAMs at temperatures <200 K, results in the molecules becoming trapped into local minima manifested by unstable tilt domains. Relaxation at temperatures >300 K introduces significant gauche defects into the SAM. Therefore, we have chosen to relax the system at 200 K, where the molecules have enough kinetic energy to overcome the local minima without introducing notable structural defects. During the relaxation, the molecules spontaneously choose the corresponding optimized geometries on which the dynamics was performed. The dynamical data were collected on the relaxed SAM structures at different temperatures (200, 250, and 300 K) for 10 ns, as well as during the annealing process with the 10 K/ns temperature rate. The structural parameters of the monolayer are calculated using the constant temperature regions of the simulation. For example, the average twists at 200 K (Figure 6) and 250 K (Figure S7) are calculated from the dynamical data between 0-10 and 15-25 ns, respectively, as shown in the time-temperature profile on the bottom part of Figure 3.

ASSOCIATED CONTENT

Supporting Information

The Supporting Information is available free of charge at https://pubs.acs.org/doi/10.1021/acsomega.0c01111.

Larger eye-cross version of Figure 1; discussion of alkyl chain twist angle measurements by IRRAS; gauche fraction definition; FF parameters; structure of different models of the Au-S interface; spatial distribution of molecular height at 250 K; average height of the basis molecules for the models at 250 K; comparison of basis molecule average height, SD, and SDOM at 200 and 250 K; spatial distribution of the folded twist at 250 K; and

structure of the SAM for $(\sqrt{3} \times \sqrt{3})R30^{\circ}$ adsorption sites in the RCP coordinate frame (PDF)

AUTHOR INFORMATION

Corresponding Author

Lloyd A. Bumm — Homer L. Dodge Department of Physics and Astronomy, University of Oklahoma, Norman, Oklahoma 73019, United States; orcid.org/0000-0003-2301-8193; Email: bumm@ou.edu

Authors

Soumya Bhattacharya — Homer L. Dodge Department of Physics and Astronomy, University of Oklahoma, Norman, Oklahoma 73019, United States; orcid.org/0000-0001-8544-3174

Mitchell P. Yothers — Homer L. Dodge Department of Physics and Astronomy, University of Oklahoma, Norman, Oklahoma 73019, United States

Liangliang Huang — School of Chemical, Biological and Materials Engineering, University of Oklahoma, Norman, Oklahoma 73019, United States; orcid.org/0000-0003-2358-9375

Complete contact information is available at: https://pubs.acs.org/10.1021/acsomega.0c01111

Author Contributions

All authors contributed equally.

Notes

The authors declare no competing financial interest.

ACKNOWLEDGMENTS

We acknowledge support from NSF CHE-1710102. Allocation time for MD simulations was performed using the Extreme Science and Engineering Discovery Environment (XSEDE) Stampede2 at the Texas Advanced Computing Center through allocation TG-CHE170067 and the OU Supercomputing Center for Education & Research (OSCER) at the University of Oklahoma (OU). S.B. acknowledges the Carl. T. Bush Fellowship and Homer L. Dodge Fellowship for support. We gratefully acknowledge the support of NVIDIA Corporation with the donation of the Tesla K40 GPU used for this research. Authors also wish to thank D. K. Ferry, D. Nematollahi, and G. Zhou for helpful discussions.

REFERENCES

- (1) Nuzzo, R. G.; Allara, D. L. Adsorption of Bifunctional Organic Disulfides on Gold Surfaces. *J. Am. Chem. Soc.* **1983**, *105*, 4481–4483. (2) Casalini, S.; Bortolotti, C. A.; Leonardi, F.; Biscarini, F. Self-Assembled Monolayers in Organic Electronics. *Chem. Soc. Rev.* **2017**, *46*, 40–71.
- (3) Love, J. C.; Estroff, L. A.; Kriebel, J. K.; Nuzzo, R. G.; Whitesides, G. M. Self-Assembled Monolayers of Thiolates on Metals as a Form of Nanotechnology. *Chem. Rev.* **2005**, *105*, 1103–1170.
- (4) Tarlov, M. J.; Burgess, D. R. F.; Gillen, G. UV Photopatterning of Alkanethiolate Monolayers Self-Assembled on Gold and Silver. *J. Am. Chem. Soc.* **1993**, *115*, 5305–5306.
- (5) Hartwich, J.; Dreeskornfeld, L.; Heisig, V.; Rahn, S.; Wehmeyer, O.; Kleineberg, U.; Heinzmann, U. STM Writing of Artificial Nanostructures in Ultrathin PMMA and SAM Resists and Subsequent Pattern Transfer in a Mo/Si Multilayer by Reactive Ion Etching. *Appl. Phys. A: Mater. Sci. Process.* 1998, 66, S685—S688.
- (6) Magnussen, O. M.; Vogt, M. R.; Scherer, J.; Behm, R. J. Double-Layer Structure, Corrosion and Corrosion Inhibition of Copper in

- Aqueous Solution. Appl. Phys. A: Mater. Sci. Process. 1998, 66, S447-
- (7) Fujihira, M.; Tani, Y.; Furugori, M.; Akiba, U.; Okabe, Y. Chemical Force Microscopy of Self-Assembled Monolayers on Sputtered Gold Films Patterned by Phase Separation. Ultramicroscopy 2001, 86, 63-73.
- (8) Schilardi, P. L.; Azzaroni, O.; Salvarezza, R. C. A Novel Application of Alkanethiol Self-Assembled Monolayers in Nanofabrication: Direct Molding and Replication of Patterned Conducting Masters. Langmuir 2001, 17, 2748-2752.
- (9) Klutse, C. K.; Mayer, A.; Wittkamper, J.; Cullum, B. M. Applications of Self-Assembled Monolayers in Surface-Enhanced Raman Scattering. J. Nanotechnol. 2012, 2012, 1-10.
- (10) Justin Gooding, J. J.; Brynn Hibbert, D. The Application of Alkanethiol Self-Assembled Monolayers to Enzyme Electrodes. TrAC, Trends Anal. Chem. 1999, 18, 525-533.
- (11) Celestin, M.; Krishnan, S.; Bhansali, S.; Stefanakos, E.; Goswami, D. Y. A Review of Self-Assembled Monolayers as Potential Terahertz Frequency Tunnel Diodes. Nano Res. 2014, 7, 589-625.
- (12) Vericat, C.; Vela, M. E.; Benitez, G.; Carro, P.; Salvarezza, R. C. Self-assembled monolayers of thiols and dithiols on gold: new challenges for a well-known system. Chem. Soc. Rev. 2010, 39, 1805-
- (13) Mete, E.; Yortanlı, M.; Danışman, M. F. A van der Waals DFT Study of Chain Length Dependence of Alkanethiol Adsorption on Au(111): Physisorption vs. Chemisorption. Phys. Chem. Chem. Phys. 2017, 19, 13756-13766.
- (14) Smith, R. K.; Reed, S. M.; Lewis, P. A.; Monnell, J. D.; Clegg, R. S.; Kelly, K. F.; Bumm, L. A.; Hutchison, J. E.; Weiss, P. S. Phase Separation within a Binary Self-Assembled Monolayer on Au{111} Driven by an Amide-Containing Alkanethiol. J. Phys. Chem. B 2001, 105, 1119-1122.
- (15) Zhou, C.; Walker, A. V. Dependence of Patterned Binary Alkanethiolate Self-Assembled Monolayers on "UV-Photopatterning" Conditions and Evolution with Time, Terminal Group, and Methylene Chain Length. Langmuir 2006, 22, 11420-11425.
- (16) Hanke, F.; Björk, J. Structure and Local Reactivity of the Au(111) Surface Reconstruction. Phys. Rev. B: Condens. Matter Mater. Phys. 2013, 87, 235422-235426.
- (17) Poirier, G. E.; Pylant, E. D. The Self-Assembly Mechanism of Alkanethiols on Au(111). Science 1996, 272, 1145-1148.
- (18) Pensa, E.; Cortés, E.; Corthey, G.; Carro, P.; Vericat, C.; Fonticelli, M. H.; Benítez, G.; Rubert, A. A.; Salvarezza, R. C. The Chemistry of the Sulfur-Gold Interface: In Search of a Unified Model. Acc. Chem. Res. 2012, 45, 1183-1192.
- (19) Wang, Y.; Solano Canchaya, J. G.; Dong, W.; Alcamí, M.; Busnengo, H. F.; Martín, F. Chain-Length and Temperature Dependence of Self-Assembled Monolayers of Alkylthiolates on Au(111) and Ag(111) Surfaces. J. Phys. Chem. A 2014, 118, 4138-4146.
- (20) Wang, Y.; Solano-Canchaya, J. G.; Alcamí, M.; Busnengo, H. F.; Martín, F. Commensurate Solid-Solid Phase Transitions in Self-Assembled Monolayers of Alkylthiolates Lying on Metal Surfaces. J. Am. Chem. Soc. 2012, 134, 13224-13227.
- (21) Mar, W.; Klein, M. L. Molecular Dynamics Study of the Self-Assembled Monolayer Composed of S(CH₂)₁₄CH₃ Molecules Using an All-Atoms Model. Langmuir 1994, 10, 188-196.
- (22) Hautman, J.; Klein, M. L. Simulation of a Monolayer of Alkyl Thiol Chains. J. Chem. Phys. 1989, 91, 4994-5001.
- (23) Hautman, J.; Klein, M. L. Molecular dynamics simulation of the effects of temperature on a dense monolayer of long-chain molecules. J. Chem. Phys. 1990, 93, 7483.
- (24) Li, T.-W.; Chao, I.; Tao, Y.-T. Relationship between Packing Structure and Headgroups of Self-Assembled Monolayers on Au(111): Bridging Experimental Observations through Computer Simulations. J. Phys. Chem. B 1998, 102, 2935-2946.
- (25) Camillone, N.; Chidsey, C. E. D.; Liu, G.-y.; Scoles, G. Superlattice Structure at the Surface of a Monolayer of Octadecane-

- thiol Self-Assembled on Au(111). J. Chem. Phys. 1993, 98, 3503-
- (26) Nuzzo, R. G.; Dubois, L. H.; Allara, D. L. Fundamental Studies of Microscopic Wetting on Organic Surfaces. 1. Formation and Structural Characterization of a Self-Consistent Series of Polyfunctional Organic Monolayers. J. Am. Chem. Soc. 1990, 112, 558-569.
- (27) Nuzzo, R. G.; Korenic, E. M.; Dubois, L. H. Studies of the Temperature-Dependent Phase Behavior of Long Chain n-Alkyl Thiol Monolayers on Gold. J. Chem. Phys. 1990, 93, 767-773.
- (28) Ulman, A. Formation and Structure of Self-Assembled Monolayers. Chem. Rev. 1996, 96, 1533-1554.
- (29) Ulman, A.; Eilers, J. E.; Tillman, N. Packing and molecular orientation of alkanethiol monolayers on gold surfaces. Langmuir **1989**, *5*, 1147-1152.
- (30) Wang, J.-G.; Selloni, A. The $c(4 \times 2)$ Structure of Short- and Intermediate-Chain Length Alkanethiolate Monolayers on Au(111): A DFT Study. J. Phys. Chem. C 2007, 111, 12149-12151.
- (31) Voznyy, O.; Dubowski, J. J. $c(4 \times 2)$ Structures of Alkanethiol Monolayers on Au (111) Compatible with the Constraint of Dense Packing. Langmuir 2009, 25, 7353-7358.
- (32) Longo, G. S.; Bhattacharya, S. K.; Scandolo, S. A Molecular Dynamics Study of the Role of Adatoms in SAMs of Methylthiolate on Au(111): A New Force Field Parameterized from Ab Initio Calculations. J. Phys. Chem. C 2012, 116, 14883-14891.
- (33) Grönbeck, H.; Häkkinen, H.; Whetten, R. L. Gold-Thiolate Complexes Form a Unique $c(4 \times 2)$ Structure on Au(111). J. Phys. Chem. C 2008, 112, 15940-15942.
- (34) Cossaro, A.; Mazzarello, R.; Rousseau, R.; Casalis, L.; Verdini, A.; Kohlmeyer, A.; Floreano, L.; Scandolo, S.; Morgante, A.; Klein, M. L.; Scoles, G. X-ray Diffraction and Computation Yield the Structure of Alkanethiols on Gold(111). Science 2008, 321, 943-946.
- (35) Chaudhuri, A.; Lerotholi, T. J.; Jackson, D. C.; Woodruff, D. P.; Jones, R. G. $(2\sqrt{3}\times3)$ rect Phase of Alkylthiolate Self-Assembled Monolayers on Au(111): A Symmetry-Constrained Structural Solution. Phys. Rev. B: Condens. Matter Mater. Phys. 2009, 79, 195439.
- (36) Wang, Y.; Chi, Q.; Zhang, J.; Hush, N. S.; Reimers, J. R.; Ulstrup, J. Chain-Branching Control of the Atomic Structure of Alkanethiol-Based Gold-Sulfur Interfaces. J. Am. Chem. Soc. 2011, 133, 14856-14859.
- (37) Wang, Y.; Chi, Q.; Hush, N. S.; Reimers, J. R.; Zhang, J.; Ulstrup, J. Gold Mining by Alkanethiol Radicals: Vacancies and Pits in the Self-Assembled Monolayers of 1-Propanethiol and 1-Butanethiol on Au(111). J. Phys. Chem. C 2011, 115, 10630-10639.
- (38) Chaudhuri, A.; Lerotholi, T. J.; Jackson, D. C.; Woodruff, D. P.; Jones, R. G. $(2\sqrt{3}\times3)$ Rect. Phase of Alkylthiolate Self-Assembled Monolayers on Au(111): A Symmetry-Constrained Structural Solution. Phys. Rev. B: Condens. Matter Mater. Phys. 2009, 79, 195439-195447.
- (39) Meena Devi, J. A Simulation Study on the Thermal and Wetting Behavior of Alkane Thiol SAM on Gold (111) Surface. Prog. Nat. Sci.: Mater. Int. 2014, 24, 405-411.
- (40) Nuzzo, R. G.; Korenic, E. M.; Dubois, L. H. Studies of the Temperature-Dependent Phase Behavior of Long Chain n-Alkyl Thiol Monolayers on Gold. J. Chem. Phys. 1990, 93, 767-773.
- (41) Bensebaa, F.; Ellis, T. H.; Badia, A.; Lennox, R. B. Thermal Treatment of n-Alkanethiolate Monolayers on Gold, As Observed by Infrared Spectroscopy. Langmuir 1998, 14, 2361-2367.
- (42) Dubois, L. H.; Nuzzo, R. G. Synthesis, Structure, and Properties of Model Organic Surfaces. Annu. Rev. Phys. Chem. 1992, 43, 437-
- (43) Poirier, G. E.; Tarlov, M. J. The c(4×2) Superlattice of n-Alkanethiol Monolayers Self-Assembled on Au(111). Langmuir 1994, 10, 2853-2856.
- (44) Lüssem, B.; Müller-Meskamp, L.; Karthäuser, S.; Waser, R. A New Phase of the $c(4 \times 2)$ Superstructure of Alkanethiols Grown by Vapor Phase Deposition on Gold. Langmuir 2005, 21, 5256-5258.
- (45) Porter, M. D.; Bright, T. B.; Allara, D. L.; Chidsey, C. E. D. Spontaneously Organized Molecular Assemblies. 4. Structural Characterization of n-Alkyl Thiol Monolayers on Gold by Optical

- Ellipsometry, Infrared Spectroscopy, and Electrochemistry. J. Am. Chem. Soc. 1987, 109, 3559-3568.
- (46) Strong, L.; Whitesides, G. M. Structures of Self-Assembled Monolayer Films of Organosulfur Compounds Adsorbed on Gold Single Crystals: Electron Diffraction Studies. *Langmuir* **1988**, *4*, 546–558.
- (47) Laibinis, P. E.; Whitesides, G. M.; Allara, D. L.; Tao, Y. T.; Parikh, A. N.; Nuzzo, R. G. Comparison of the Structures and Wetting Properties of Self-Assembled Monolayers of *n*-Alkanethiols on the Coinage Metal Surfaces, Copper, Silver, and Gold. *J. Am. Chem. Soc.* 1991, 113, 7152–7167.
- (48) Bareman, J. P.; Klein, M. L. Collective Tilt Behavior in Dense, Substrate-Supported Monolayers of Long-Chain Molecules: A Molecular Dynamics Study. *J. Phys. Chem.* **1990**, *94*, 5202–5205.
- (49) Fenter, P.; Eisenberger, P.; Liang, K. S. Chain-Length Dependence of the Structures and Phases of $CH_3(CH_2)_{n-1}SH$ Self-Assembled on Au(111). *Phys. Rev. Lett.* **1993**, 70, 2447–2450.
- (50) Ulman, A. An Introduction to Ultrathin Organic Films; Academic: Boston, 1991.
- (51) Ulman, A. Formation and Structure of Self-Assembled Monolayers. Chem. Rev. 1996, 96, 1533–1554.
- (52) Plimpton, S. Fast Parallel Algorithms for Short-Range Molecular Dynamics. *J. Comput. Phys.* **1995**, *117*, 1–19.
- (53) Murzyn, K.; Bratek, M.; Pasenkiewicz-Gierula, M. Refined OPLS All-Atom Force Field Parameters for *n*-Pentadecane, Methyl Acetate, and Dimethyl Phosphate. *J. Phys. Chem. B* **2013**, *117*, 16388–16396.
- (54) Ryckaert, J.-P.; Klein, M. L.; McDonald, I. R. Computer Simulations and the Interpretation of Incoherent Neutron Scattering Experiments on the Solid Rotator Phases of Long-Chain Alkanes. *Mol. Phys.* **1994**, *83*, 439–458.

Supporting Information

Interaction of the $(2\sqrt{3} \times 3)$ rect. Adsorption-Site Basis and Alkyl-Chain Close Packing in Alkanethiol Self-Assembled Monolayers on Au(111): A Molecular Dynamics Study of Alkyl-Chain Conformation

Soumya Bhattacharya†, Mitchell P. Yothers†, Liangliang Huang#, and Lloyd A. Bumm†*

†Homer L. Dodge Department of Physics and Astronomy, University of Oklahoma, Norman, OK, 73019

#School of Chemical, Biological and Materials Engineering, University of Oklahoma, Norman, OK, 73019

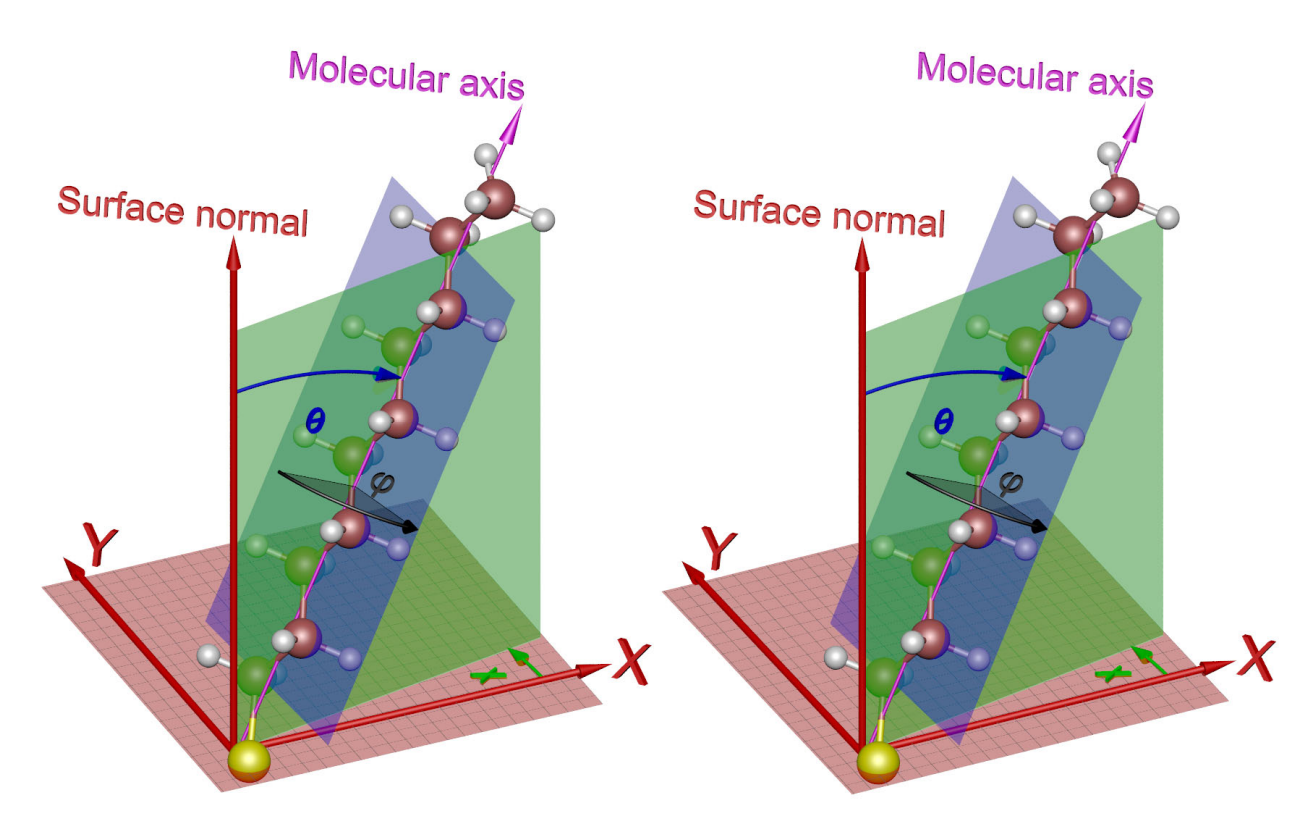


Figure S1. The eye-cross stereo image pair of the molecular geometry. In this alkyl-chain centric model the molecular axis passes through the origin where it intersects the surface. The tilt angle (θ) is defined by the angle between the surface normal and the axis of the molecular (molecular axis). The twist of the molecular backbone (φ) is defined by the angle between the tilt plane (green plane) containing the surface normal and the molecular axis and the plane of the carbon atoms (blue plane, the molecular plane). Zero twist angle is defined where these two planes coincide and the bond between the head group and alpha methylene makes the largest angle with respect to the surface normal $(\alpha$ -CH₂ is closer to the substrate). The twist angle increases positively in the counterclockwise direction while looking down the molecular axis (right-handed coordinate system). The direction of the tilt (χ) is the angle between the positive x-axis and the projection of the molecular axis on the plane of the substrate (xy-plane).

A. Discussion of alkyl chain twist angles measurements by infrared reflection absorption spectroscopy (IRRAS)

The principle experimental measurements of the twist of the alkyl-chain plane (φ) in SAMs come from IRRAS. Nuzzo et al.¹⁻² use a single-chain per unit-cell model and report a twist angle of 55°. The most recent study of Laibinis et al.³ followed up the previous work using a two-chain per unit-cell model and report twist angles of -48° and $+50^{\circ}$. We use this latter work for comparison to our simulations. Because a clear and consistent definition of the molecular twist angle is critical for comparison of simulation and experiment, and because the definition of φ (and its zero) in ref. 3 is muddied by the introduction of positive and negative tilt angles, we will discuss the definition in detail for further clarification.⁴ We also justify our interpretation of the reported twist angles as $\varphi = +132^{\circ}$ and $+50^{\circ}$, based on the inherent symmetries and the discussion in ref. 3.

The molecular geometry of an all-trans alkane chain can be visualized by applying three rotations to the molecule. We begin with the molecule standing straight up on the surface (xyplane) with the alkyl-chain axis (molecular axis) aligned with the surface normal (z-axis). The alkyl plane aligned with the xz-plane, with the projection of the S to α -CH₂ bond vector pointing in the +x-direction. This standing up conformation of the molecule corresponds to zero tilt (θ = 0°) and zero twist (φ = 0°). Now, rotation of the standing up alkane chain about its molecular axis (z-axis) in the counterclockwise direction (while looking down the molecular axis toward the surface) introduces positive twist. The tilt of a molecule is achieved by rotation of the molecular axis about the y-axis where tilting towards the +x-axis is described as a positive tilt. For tilt direction (χ), the tilted molecule is again rotated around the z-axis (rotation from +x-axis to +y-axis is defined as the positive χ). Stated another way, the angles are defined using the right-handed coordinate convention.

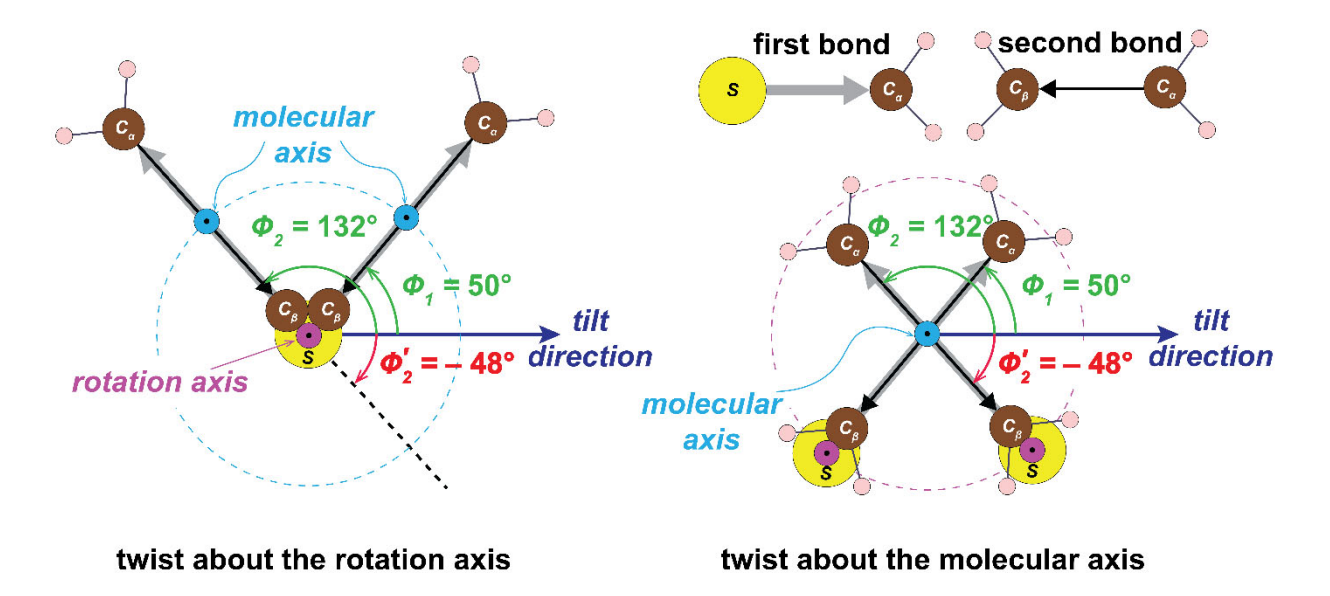


Figure S2. The molecular twist in two different reference frames. Left) The view in the frame of the physical rotation, looking down the rotation axis with the sulfur fixed on the surface. The β -CH₂ hydrogens are left out for clarity. Right) The view in the frame of the molecular axis, looking down the chain. Changing the twist causes the molecular axis to precess around the rotation axis. The sulfur to α -CH₂ vector shown as the thick gray arrow. The α -CH₂ to β -CH₂ vector is show as the thin black arrow. The two twist angles from Laibinis et. al. are depicted.³

Figure S2 shows two views of the molecular twist looking along the physical rotation axis (Figure 2, Left) and the molecular axis (Figure 2, Right). The twist of a chain is defined by the relative orientation of the carbon plane and the tilt plane, as shown in Figure S1. For an all-trans chain in this projection, the twist angle is defined by the angle between the tilt direction and the first bond (S- α CH₂). With the sulfur fixed on the surface, changing the twist angle causes the molecular axis to precess around the sulfur. Changing the twist also changes the Au-S-CH₂ bond angle. Twisting a single chain within a SAM would also change its distance to neighboring chains. We depict two twist angles, $\varphi = +132^{\circ}$ and $+50^{\circ}$ (see the discussion below).

For a full understanding of the reported φ values in ref. 3, we need to discuss the basics of the IRRAS measurement and how φ is determined. IRRAS is sensitive to the orientation of the transition dipole of the mode in the monolayer. The component of the transition dipole normal to the metallic substrate (Au(111) in our case) contributes to the IRRAS absorption, while the parallel component to the substrate is strongly suppressed. Consequently, the observed intensity varies with the cosine square of the angle of the mode with the surface normal. The angle of the mode to the surface normal can be obtained by comparing the intensity in the film to that of a suitable reference phase. Typically, a polycrystalline solid phase alkanethiol or disulfide has been used, which has alkyl chain conformations and molecular environment closely related to that found in SAMs. This approach also relies on the assumption that the transition dipole strength in the SAM is the same as that in the reference phase. This assumption has been shown to work well for the methylene stretching modes, but not so well for the methyl stretching modes.

The infrared modes used to measure the chain twist are those of the d^+ and d^- methylene stretching. These two modes and the molecular axis are mutually orthogonal. The d^+ involves the CH₂ symmetric stretching, where the stretching vibration of the odd and even CH₂s are 180° out of phase—antisymmetric in the plane of the chain. The d^- involves the CH₂ antisymmetric stretching, where the stretching vibration of the odd and even CH₂s are in phase—antisymmetric out of the plane of the chain. For a given tilt angle, the d^+ intensity will be maximum at $\varphi = 0^\circ$ and 180° and zero at 90° and 270°. The d^- intensity is offset by 90°, with maximum at $\varphi = 90^\circ$ and 270° and zero at 0° and 180°. These properties give the mode intensities C₂ symmetry about the molecular axis ($\varphi = \varphi + 180^\circ$) as well as two mirror planes—the tilt plane ($\varphi = -\varphi$) and the plane perpendicular to the tilt plane containing the molecular axis ($\varphi = 180^\circ - \varphi$). As a result,

methylene modes alone cannot distinguish between symmetry equivalent twists, i.e. $\varphi = -50^{\circ}$, $+50^{\circ}$, $+130^{\circ}$, and -130° will have the same d⁺ and d⁻ intensities.

The three methyl stretching modes have different symmetry with respect to the twist angle and should in principle further constrain the twist angle. The r⁺ symmetric stretch is oriented along the CH₂-CH₃ bond. The r_a antisymmetric stretch is perpendicular to the CH₂-CH₃ bond and in the plane of the alkyl chain. The r_b antisymmetric stretch is perpendicular to the CH₂-CH₃ bond and perpendicular to the plane of the alkyl chain. Unlike the symmetry of the methylene modes, the methyl r⁺ and r_a modes possess only mirror plane symmetry—the tilt plane ($\varphi = -\varphi$). The r_b mode has the same symmetry as the methylene d⁻ mode. The lower symmetry of the methyl modes could further constrain the twist angle within the tilt-plane mirror symmetry. Twist angles in the range 90° to 270° (through 180°) orient the CH₂-CH₃ bond more normal to the surface increasing the intensity of r⁺ mode and decreasing the intensity of r_a mode. Whereas twist angles in the range -90° to +90° (through 0°) orient the CH₂-CH₃ bond more parallel to the surface increasing the intensity of r_a mode and decreasing the intensity of r⁺ mode. Therefore, these two modes can be used to distinguish twists related by C2 symmetry about the molecular axis and mirror symmetry about the plane perpendicular to the tilt plane containing the molecular axis. However, the methyl modes are complicated by Fermi resonances and the intensities in the SAM do not correspond as well with the reference phase as do the methylene modes. Since the methyl mode intensities do not correspond well to the reference phase, good fits for CH2 and CH3 modes could not be achieved by twisting the molecule alone. In addition, the $r_{\bar{b}}$ is weaker in the SAM and appears as a shoulder on the stronger r_a , thus not as useful for molecular orientation. Therefore, more interpretation was required.

Given these symmetries, it is perplexing why Laibinis et al. report $\varphi = -48^{\circ}$ and $+50^{\circ}$, which should be practically indistinguishable from the methylene and methyl modes. They use two

arguments to guide their interpretation. First, the observed odd-even methyl-mode intensity oscillation. Second, the hypothesis that the surface-S-CH₂ bond orientation and/or torsion angles should be the same for all the molecules. The latter is quite reasonable from the prevailing view at the time, that all the molecules had the same adsorption site, but is not generally the case for the models we consider in our work presented here. Below, we discuss the former line of reasoning.

The intensity of the r⁺ mode is observed to be strongest for even-length chains and lower for odd-length chains. The r_a^- mode displays the opposite odd-even dependence. The conclusion is that the CH₂-CH₃ bond is more normal to the surface for even than for odd.⁵ This supports the hypothesis that the twist angle is in the range -90° to $+90^{\circ}$. However, their models over predict the magnitude of the oscillation by factor of 2–3 (ref. 3, Figure 5). Nevertheless, they say the two twist angles were restricted to the range of -90° to $+90^{\circ}$ for their fitting. This was argued as satisfying the "methyl surface corrugation" (ref. 3 footnote 43), which we presume to mean the orientation of the methyl groups. This choice of twist angles has the effect of increasing r⁺ at the expense of ra. Reasonable fits of the methyl modes required assuming 45% gauche fraction of the C-C-C-CH₃ bond. That equally good fits could have been obtained choosing instead $\varphi = +132^{\circ}$ and +50° seems likely given the data shown in (ref. 3, Figures 8 and 9). Although that choice would make the surface-S-CH₂ bond orientation and/or torsion angles different for the two twist classes. There is also a logical inconsistency in the discussion of the angular difference between the two twist angles. The discussion concludes the difference should be 82°, but the difference between the reported angles is 98°. The choice of $\varphi = +132^{\circ}$ and $+50^{\circ}$ would satisfy the 82° difference.

B. Gauche fraction definition

In the all-trans configuration of the alkyl chain, all the carbon atoms lie on a plane—the molecular plane (Figure S1, blue plane). Thermal motion causes the carbon atoms to deviate from the all-trans molecular plane. Excursions of each C–C–C bond dihedral angle (Ψ) from the trans energy well into the adjacent gauche wells can be quantified by the gauche fraction.

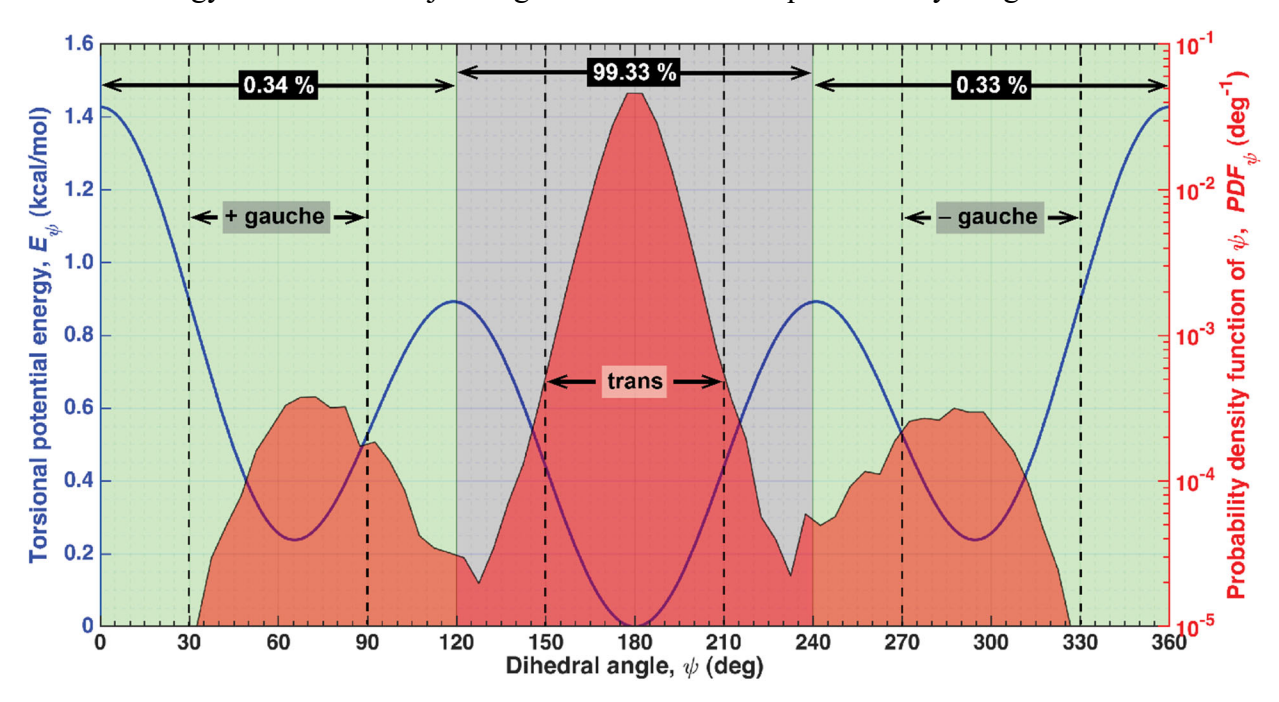


Figure S3. The C–C–C dihedral potential energy (E_{Ψ}) term is plotted against the dihedral angle (Ψ) on the left y-axis. The trans and two gauche conformations are noted. On the right y-axis, we plotted the probability density function of the dihedral angle (PDF_{Ψ}) for model A at 200 K. We use semi-log axis for PDF_{Ψ} to better illustrate the gauche population as gauche population is significantly smaller than the trans population.

The torsion around the $C_{i-1}C_{i+1}$ bond is characterized by the $C_{i-1}-C_i-C_{i+1}-C_{i+2}$ dihedral angle, defined by the angle between the planes containing C_{i-1}, C_i, C_{i+1} and C_i, C_{i+1}, C_{i+2} where the anticlockwise rotation of the $C_{i+1}-C_{i+2}$ bond about the C_i-C_j bond defines the positive increment

of Ψ keeping the C_{i-1} – C_i bond unchanged. For a C10 molecule the index i runs from 1 to 8, where C_1 is the alpha carbon and C_0 is the sulfur.

The C-C-C dihedral potential ($E_{\mathcal{V}}$) is shown in Figure S3 (left vertical axis), with the parameters given in Table S3. There is a global energy minimum at 180° (trans, antiperiplanar) and two local minima at 65° and 295° (gauche, synclinal).⁶ The C-C-C bond conformation is termed trans (all four carbon atoms lie on a plane) when $150^{\circ} \le \Psi \le 210^{\circ}$ corresponding to the minimum energy configuration of Ψ . Deviation from the trans conformation could result in one of the two gauche conformations namely positive gauche (+gauche) and negative gauche (-gauche) and they are defined as follows: for +gauche, $30^{\circ} \le \Psi \le 90^{\circ}$ and for -gauche, $270^{\circ} \le \Psi \le 330^{\circ}$.⁷

The Ψ probability density function (PDF_{Ψ}) for model A at 200 K is overlaid in Figure S3 (right vertical axis) showing the distribution of dihedral angles. The semi-log PDF_{Ψ} plot shows most of the dihedral angles lie in the trans well (99.33 %) with a very small population in the gauche wells (0.67 %), i.e. molecules are predominantly trans in the monolayer. Consistent with previous studies, most of the gauche conformations reside at the surface. The terminal dihedral bonds have a 4.5% gauche fraction, which is 85% of the gauche population in the monolayer. Note the local maxima of the PDF_{Ψ} for the gauche conformations does not occur at the gauche potential energy minima, but is biased towards the trans conformation side of the wells. This is because the molecules are also subject to C-C-C-H and H-C-C-H dihedral potentials— PDF_{Ψ} is a system property.

For the purpose of characterizing the gauche fraction, dihedral angles 0–120° are counted as +gauche and 240–360°, as -gauche, corresponding to the potential energy wells, shown as two green regions in Figure S3. The gauche fraction presented in the paper (Figure 3) is calculated as follows:

$$\frac{N_{+gauche} + N_{-gauche}}{N_{total}} \times 100\%$$
 .

Here $N_{+gauche}$, $N_{-gauche}$, and N_{total} are the population of the dihedral angle in the positive and negative gauche regions and the total population of the C-C-C dihedral angle respectively. Such that $N_{total} = N_{+gauche} + N_{-gauche} + N_{trans}$.

C. Force field parameters

Bond stretching: $K_r (r - r_0)^2$

Table S1. Force Field Parameters for Bond Stretching

Bond	<i>ro</i> (Å)	K_r (kcal/ mol Å ²)
S-C ⁹	1.81	222
C-H ¹⁰	1.09	340
C-C ¹⁰	1.529	268

Bond bending: $K_{\theta} (\theta - \theta_{\theta})^2$

Table S2. Force Field Parameters for Bond Bending

Bond Angle	θ _θ (°)	K_{θ} (kcal/ mol rad ²)
∠S-C-C ⁹	114.7	50.0
∠C-C-C ¹⁰	112.7	58.35
∠C-C-H ¹⁰	110.7	37.5
∠H-C-H ¹⁰	107.8	33.0

Dihedral angle vibration: $\frac{1}{2}K_{\phi}^{1}(1+\cos\phi)+\frac{1}{2}K_{\phi}^{2}(1-\cos2\phi)+\frac{1}{2}K_{\phi}^{3}(1+\cos3\phi)$

Table S3. Fourier Components of the Dihedral Angles

Dihedral Angle	K_{ϕ}^{1} (kcal/mol)	K_{ϕ}^{2} (kcal/mol)	K_{ϕ}^{3} (kcal/mol)
C-C-C ¹¹	0.528	-0.186	0.900
C-C-C-H ¹²	0	0	0.366
H-C-C-H ¹¹	0	0	0.150

Non-bonded interaction:
$$4\varepsilon \left\{ \left(\frac{\sigma}{r}\right)^{12} - \left(\frac{\sigma}{r}\right)^{6} \right\} + C \frac{q_i q_j}{\varepsilon_0 r}$$
, where $r < r_c = 12$ Å.

Table S4. Force Field Parameters for Non-Bonded Interactions

Interaction Site	σ (Å)	ε (kcal/mol)	q_i (e)
Au _{adatom} ¹³	2.934	0.039	0
S ¹²	3.550	0.250	0
C (in CH ₂) ¹¹	3.5	0.066	-0.12
C (in CH ₃) ¹¹	3.5	0.066	-0.18
H (in CH ₂) ¹¹	2.5	0.030	0.06
H (in CH ₃) ¹¹	2.5	0.030	0.06

The cutoff distance for both the vdW interaction and the Coulombic potential is the same, 12 Å. The mixing rule used is $\varepsilon_{ij} = \sqrt{\varepsilon_i \varepsilon_j}$ and $\sigma_{ij} = \sqrt{\sigma_i \sigma_j}$. The Coulombic interaction is treated via PPPM method.

D. Structure of different models of Au-S interface

Initially, the coordinates for the sulfur and Au adatoms are taken from the references mentioned cited in (Table 1). However, due to the inconsistent $(2\sqrt{3} \times 3)$ rect. unitcell dimensions, we have rescaled all the coordinates using the Au-Au distance of 2.88376 Å. ¹⁴ The corresponding size of the unitcell is $(8.65127 \text{ Å} \times 9.98963 \text{ Å})$. All the Au/S interface models are simulated with and without the top layer of Au atoms (nominal Au(111) surface atoms). Inclusion of these Au atoms did not affect the simulation results for the SAMs, but does increase the computational expense. Thus we conclude the top-layer gold atoms are not a critical component for our MD modeling of the SAM structure, therefore not reported in Table S5. The coordinates (Å) of the sulfur atoms and the gold adatoms for each model are reported in Table S5. We have used 6 significant figures to reduce round-off errors.

Table S5. Sulfur and Gold Adatom Coordinates

Model	Adatoms	Vacancies	Coordinate of S atoms [x, y, z]	Coordinate of Au Adatoms
A	1	1	[-8.32380, 3.31830, 13.32000];	[-3.52380, 9.77170, 13.32000].
			[-4.69710, 5.39830, 13.32000];	
			[-9.65710, 8.81170, 13.92000];	
			[-5.17710, 10.89170, 13.92000].	
В	4	0	[6.47838, 3.77866, 1.36841];	[7.05530, 2.32384, -0.42612];
			[2.17786, 6.35487, 1.44976];	[2.94827, 4.95950, -0.33068];
			[6.74862, 8.15539, -0.05977];	[6.19585, 5.82202, 0.14563];
			[2.34536, 10.70081, -0.07553].	[1.85646, 8.34482, 0.12379].
С	0	0	[-6.09580, -0.95400, 14.43490];	
			[-2.38030, 1.95350, 14.09960];	N/A
			[-6.51550, 5.19760, 14.89380];	
			[-1.43590, 7.87580, 14.94380].	
D	2	0	[-2.79830, 0.22660, 5.03000];	[-2.88570, 2.49908, 5.47000];
			[-7.60550, 2.58650, 5.03000];	[-7.16840, 4.85900, 5.47000].
			[-3.32270, 4.68420, 5.03000];	
			[-7.16840, 7.04400, 5.03000].	
Е	1.2	2.8	[6.97806, 1.12880, 16.00281];	[3.40381, 6.76089, 16.38680];
			[2.65246, 3.62619, 16.00281];	[-0.92179, 6.76089, 16.38680].
			[5.29453, 5.22251, 16.70918];	
			[0.96893, 7.71989, 16.70918].	

F	4	0	[-10.09329, 5.82739, 4.80000];	[-10.09329, 5.82739, 2.40000];
			[-5.76760, 8.32483, 4.80000];	[-5.76760, 8.32483, 2.40000];
			[-10.09329, 9.15733, 4.80000];	[-10.09329, 9.15733, 2.40000];
			[-5.76760, 11.65478, 4.80000].	[-5.76760, 11.65478, 2.40000].
G	2	0	[7.52002, 2.91155, 9.87941];	[7.65434, 5.24762, 9.72556];
			[3.49748, 5.52212, 9.93266];	[3.24224, 7.84172, 9.69442].
			[8.03580, 7.56142, 9.83508];	
			[3.38609, 10.17833, 9.73591].	
Н	2	1	[7.40589, 2.86455, 9.78721];	[7.60367, 5.20053, 9.69969];
			[3.48157, 5.51290, 9.83151];	[3.20234, 7.84312, 9.64630].
			[8.04538, 7.50390, 9.84549];	
			[3.32828, 10.18725, 9.67556].	
Ι	2	1	[7.59130, 2.70457, 9.74405];	[7.55506, 5.05234, 9.64422];
			[3.48331, 5.20823, 9.80910];	[3.22828, 7.53903, 9.67939];
			[7.86329, 7.37781, 9.80354];	
			[3.22494, 9.88605, 9.80267].	
J	2	1	[7.62810, 2.73302, 9.80484];	[7.52526, 5.07040, 9.64368];
			[3.47979, 5.22554, 9.76598];	[3.17018, 7.53873, 9.59298].
			[7.79187, 7.39795, 9.73822];	
			[3.17904, 9.86675, 9.79834].	

E. Spatial distribution of molecular height at 250 K

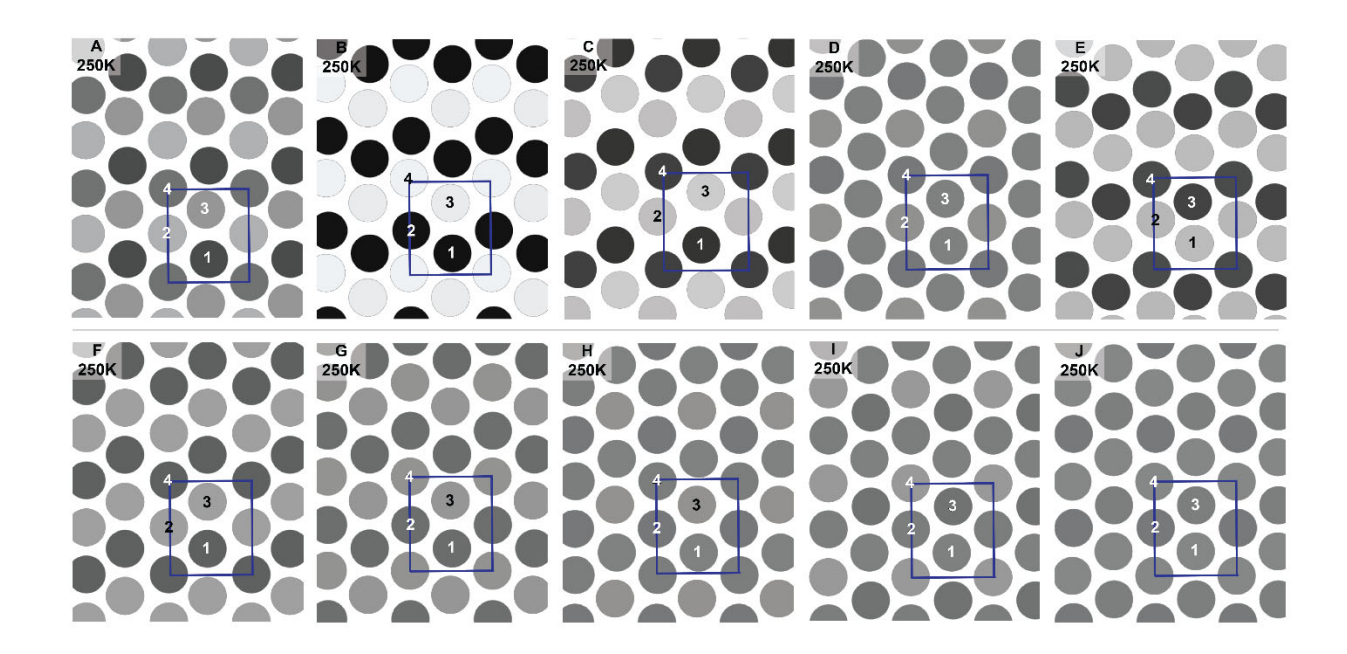


Figure S4. The spatial distribution of the height difference at the methyl interface at 250 K for models A-J. The numbering scheme for the basis types is same as that shown in Table 1 in the main paper. For better visualization, the $(2\sqrt{3} \times 3)$ rect. unit cell (blue box) is tiled 3×3 for easy visualization of the patterns. The position of the circles is the average position of the methyl groups and the color of the circle represent the average height of the molecule. The gray scale is kept the same for all the models for better comparison, the higher molecules are represented by the lighter shades.

F. Average height of the basis molecules for the models at 250 K

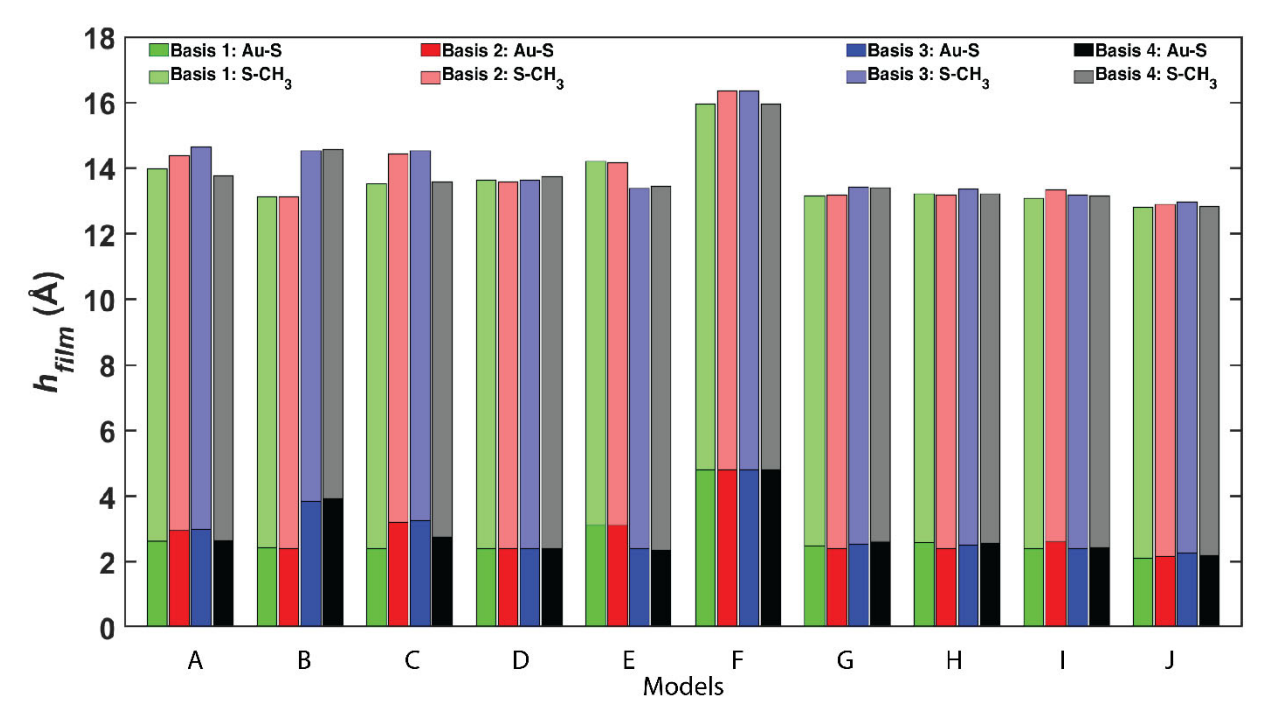


Figure S5. The average height of the four basis-type methyl-group C atoms at 250 K from the Au(111) substrate for each model separated by contribution. The darker segments (Au-S) represent the z-height of the S head groups from the Au(111) substrate, the contribution to the z-height from the S atom adsorption site. The lighter segments (S-CH₃) represent the z-height of the methyl group C atoms from the corresponding S atoms, the contribution to the z-height from the molecular conformation.

G. Comparison of basis molecule average height, SD, and SDoM at 200 and 250 K

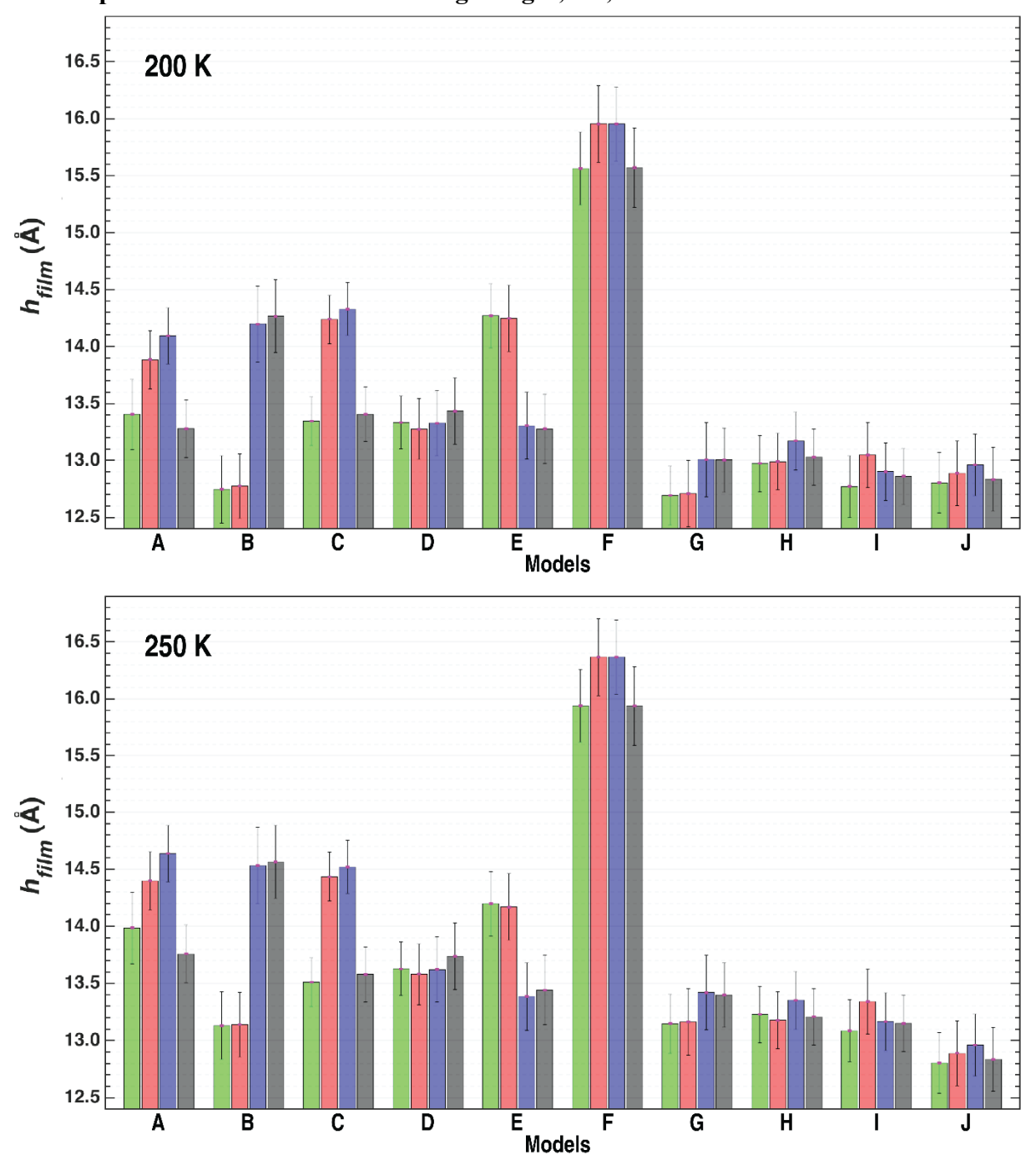


Figure S6. The standard deviation (SD) and the standard deviation of the mean (SDoM) for molecular heights are shown for each basis type for ten models. The black vertical error bars represent the SD of height, whereas the small (~50 time smaller than the SD) magenta bars shows the corresponding SDoM. Notice the height difference between 200 K and 250 K and the larger SD error bars for 250 K.

G. Spatial distribution of the folded twist at 250 K

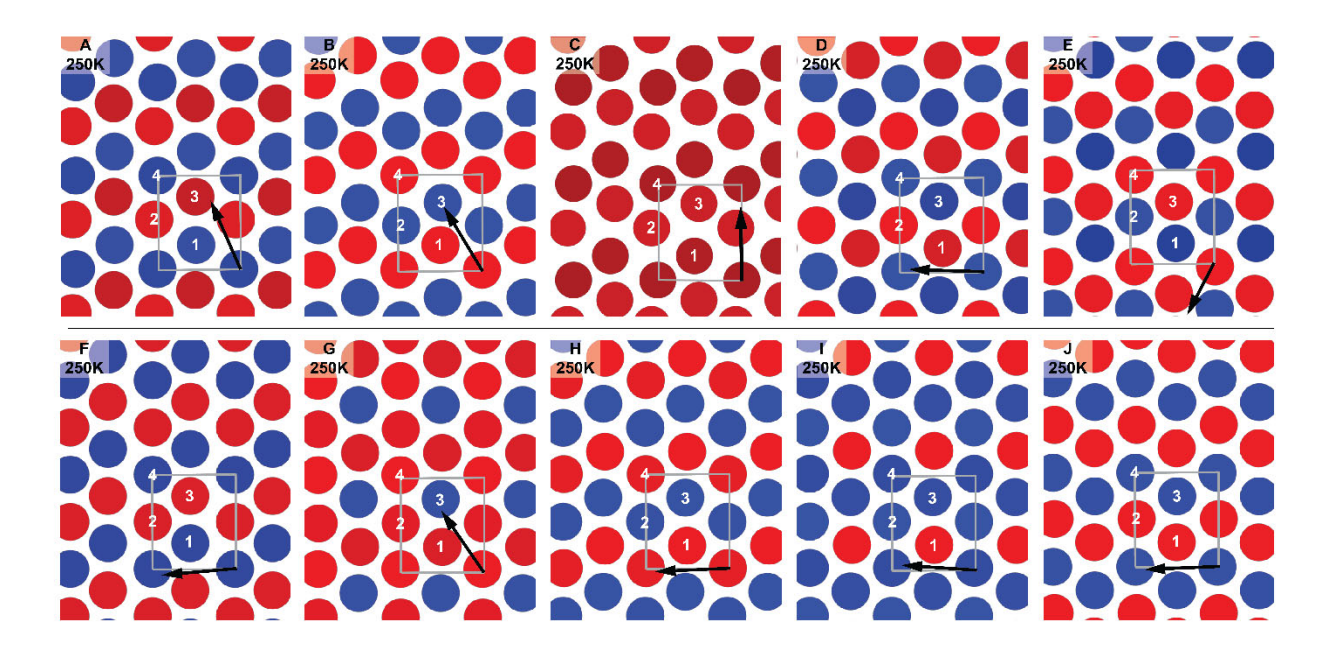


Figure S7. The spatial distribution of the molecular twist is shown for ten Au-S interfacial models at 250 K for models A-J. The position of the circles is the average position of the methyl groups, and the color of the circle represents the average value of the folded twist; Blue: $0^{\circ} \le \phi < 90^{\circ}$ and Red: $90^{\circ} \le \phi < 180^{\circ}$. The corresponding tilt direction (black arrow) and the $(2\sqrt{3} \times 3)$ rect. unit cell (gray rectangle) are shown for comparison. The numbering scheme for the basis molecules is the same as in Table 1 in the main paper. The $(2\sqrt{3} \times 3)$ rect. unit cell is tiled 3×3 for easy visualization of the patterns.

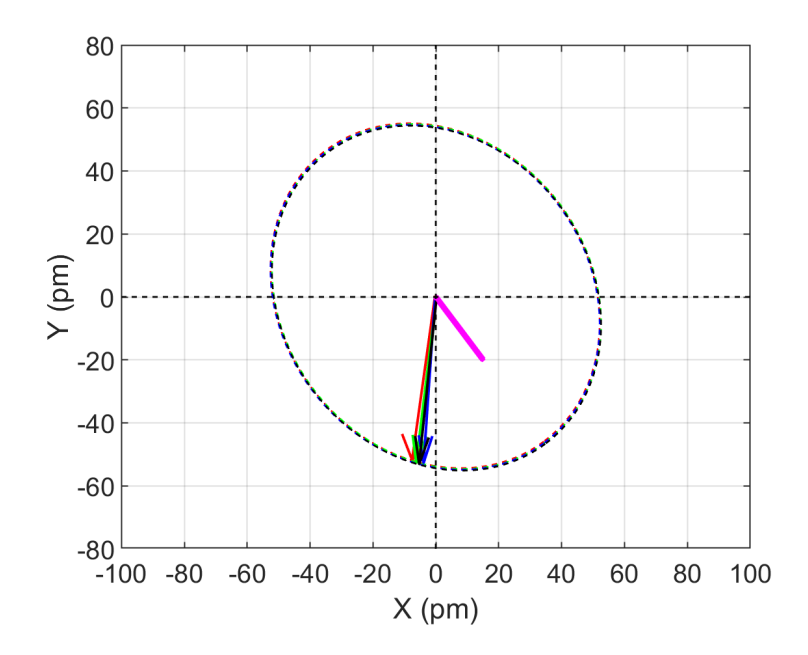


Figure S8. The alkyl chain geometry of the $(\sqrt{3} \times \sqrt{3})$ R30° reference structure in the reduced close-packed coordinate system (see main paper). The S head group positions are at the vertex of the arrow and the magenta lines. The chain axis is located at the end of the arrow. The magenta lines for each arrow indicated the chain tilt direction. The twist is the angle between the magenta line and the arrow. The dotted ellipses show the possible positions of the idealized all-trans alkyl chain axis as the twist is swept in a full circle around the S headgroup. The basis types are indicated by the color of the arrows (red = 1, green = 2, blue = 3, and black = 4).

References

- (1) Nuzzo, R. G.; Fusco, F. A.; Allara, D. L., Spontaneously Organized Molecular Assemblies. 3.

 Preparation and Properties of Solution Adsorbed Monolayers of Organic Disulfides on
 Gold Surfaces. *J. Am. Chem. Soc.* **1987**, *109* (8), 2358-2368.
- (2) Nuzzo, R. G.; Dubois, L. H.; Allara, D. L., Fundamental Studies of Microscopic Wetting on Organic Surfaces. 1. Formation and Structural Characterization of a Self-Consistent Series of Polyfunctional Organic Monolayers. J. Am. Chem. Soc. 1990, 112 (2), 558-569.
- (3) Laibinis, P. E.; Whitesides, G. M.; Allara, D. L.; Tao, Y. T.; Parikh, A. N.; Nuzzo, R. G., Comparison of the Structures and Wetting Properties of Self-Assembled Monolayers of *n*-Alkanethiols on the Coinage Metal Surfaces, Copper, Silver, and Gold. *J. Am. Chem. Soc.* **1991**, *113* (19), 7152-7167.
- (4) The molecular symmetry relates the twist at positive tilt angle with the twist at negative tilt angle: $\theta = -\theta$ and $\varphi = 180^{\circ} + \varphi$.
- (5) The discussion in Ref. 3 sometimes uses odd and even to refer to the number of methylenes $HS(CH_2)_nCH_3$ and sometimes odd-even with respect to the total number of carbon atoms $HSC_nH_{(2n+1)}$.
- (6) IUPAC. Compendium of Chemical Terminology, 2nd ed. (the "Gold Book"). Compiled by A. D. McNaught and A. Wilkinson. Blackwell Scientific Publications, Oxford (1997). XML on-line corrected version: http://goldbook.iupac.org (2006-) created by M. Nic, J. Jirat, B. Kosata; updates compiled by A. Jenkins. ISBN 0-9678550-9-8.
 https://doi.org/10.1351/goldbook.T06406.
- (7) The definition of +gauche and -gauche is more obvious when the conformation is described in terms of the torsion angle. These decribe the same angle, but the dihedral angle is

- defined between 0° and 360° with the zero at the cis conformation. The torison angle is defines between -180° and $+180^{\circ}$ with the zero at the trans conformation.
- (8) Mar, W.; Klein, M. L., Molecular Dynamics Study of the Self-Assembled Monolayer

 Composed of S(CH₂)₁₄CH₃ Molecules Using an All-Atoms Model. *Langmuir* **1994**, *10*(1), 188-196.
- (9) Weiner, S. J.; Kollman, P. A.; Nguyen, D. T.; Case, D. A., An All Atom Force Field for Simulations of Proteins and Nucleic Acids. *J. Comput. Chem.* **1986**, *7* (2), 230-252.
- (10) Kaminski, G.; Jorgensen, W. L., Performance of the AMBER94, MMFF94, and OPLS-AA Force Fields for Modeling Organic Liquids. *J. Phys. Chem.* **1996**, *100* (46), 18010-18013.
- (11) Murzyn, K.; Bratek, M.; Pasenkiewicz-Gierula, M., Refined OPLS All-Atom Force Field Parameters for *n*-Pentadecane, Methyl Acetate, and Dimethyl Phosphate. *J. Phys. Chem. B* **2013**, *117* (51), 16388-16396.
- (12) Jorgensen, W. L.; Maxwell, D. S.; Tirado-Rives, J., Development and Testing of the OPLS All-Atom Force Field on Conformational Energetics and Properties of Organic Liquids. *J. Am. Chem. Soc.* 1996, 118 (45), 11225-11236.
- (13) Meena Devi, J., A Simulation Study on the Thermal and Wetting Behavior of Alkane Thiol SAM on Gold (111) Surface. *Prog. Nat. Sci.: Mater. Int.* **2014**, *24* (4), 405-411.
- (14) Wyckoff, R. W. G., Crystal Structures. 2nd ed.; Wiley: New York, 1963; Vol. 1.